Measurement report: Long-term variations in surface NO$_X$ and SO$_2$ mixing ratios from 2006 to 2016 at a background site in the Yangtze River Delta region, China

Qingqing Yin [1], Qianli Ma[2], Weili Lin[1], Xiaobin Xu[3], Jie Yao[2]

5 [1] Key Laboratory of Ecology and Environment in Minority Areas (Minzu University of China), National Ethnic Affairs Commission, Beijing 100081, China
[2] Lin'an Atmosphere Background National Observation and Research Station, Lin'an 311307, Hangzhou, China
[3] Key Laboratory for Atmospheric Chemistry, Chinese Academy of Meteorological Sciences, Beijing 100081, China

Correspondence to: Weili Lin (linwl@muc.edu.cn)

10 **Abstract.** China has been experiencing rapid changes in emissions of air pollutants in recent decades. Increased emissions of primary particulates and reactive gases caused severe haze in several polluted regions including the Yangtze River Delta (YRD). Measures implemented in recent years for improving air quality have reduced the emissions of NO$_X$, SO$_2$, etc. The emission changes of these gases are reflected by tropospheric columns from satellite observations and surface measurements of surface concentrations from urban sites. However, little is known about the long-term variations in regional background
15 NO$_X$ and SO$_2$. In this study, we present NO$_X$ and SO$_2$ measurements from the Lin'an station (LAN, 119°44′ E,30°18′ N,138.6 m a.s.l.), one of the Global Atmosphere Watch (GAW) stations in China. We characterize the seasonal and diurnal variations and study the long-term trends of NO$_X$ and SO$_2$ mixing ratios observed at LAN from 2006 to 2016. We also interpret the observed variations and trends in term of changes in meteorological conditions as well as emission of these gases. The overall average mixing ratios of NO$_X$ (NO$_2$) and SO$_2$ during 2006–2016 were 13.6 ± 1.2 ppb (12.5 ± 4.6) and 7.0 ± 4.2 ppb, respectively.
20 The averaged seasonal variations showed maximum values of NOx and SO$_2$ in December (23.5 ± 4.4 ppb) and January (11.9 ± 6.2 ppb), respectively, and minimum values of 7.1 ± 0.8 ppb and 2.8 ± 2.3 ppb (both in July), respectively. The average diurnal variation characteristics of NO$_X$ and SO$_2$ differed considerably from each other though the daily average mixing ratios of both gases were significantly correlated ($R^2 = 0.29$, $P < 0.001$). The annual average mixing ratio of NO$_X$ increased during 2006–2011 and then decreased significantly at 0.78 ppb/yr (–5.16 %/yr, $P < 0.01$). The annual 95 % and 5 % percentiles of
25 hourly NO$_X$ mixing ratios showed upward trends until 2012 and 2014, respectively, before a clear decline. The annual average mixing ratio of SO$_2$ decreased significantly at 0.99 ppb/yr (–8.27 %/yr, $P < 0.01$) from 2006–2016. The annual 95 % and 5 % percentiles of hourly SO$_2$ mixing ratios all exhibited significant ($P < 0.001$) downward trends at 3.18 ppb/yr and 0.19 ppb/yr, respectively. Changes in the total NO$_X$ and SO$_2$ emissions as well as the industrial emissions in the YRD region were significantly correlated with the changes in annual NO$_X$ and SO$_2$ mixing ratios. The significant decreases in NO$_X$ from 2011
30 to 2016 and SO$_2$ from 2006 to 2016 highlight the effectiveness of relevant control measures on the reduction in NO$_X$ and SO$_2$ emissions in the YRD region. A decrease of annual SO$_2$/NO$_X$. ratio was found, suggesting a better efficacy in the emission reduction of SO$_2$ than NO$_X$. We found gradual changes in average diurnal patterns of NO$_X$ and SO$_2$, which could be attributed

to increasing contributions of vehicle emissions to NO_X and weakening impacts of large sources on the SO_2 concentration. This study reaffirms China's success in controlling both NO_X and SO_2 in the YRD but indicate at the same time a necessity to strengthen the NO_X emission control.

Keywords: background NO_X and SO_2; long-term trend; emission reduction.

1 Introduction

China's economy has experienced decades of rapid development, resulting in considerable pollutant emissions from coal combustion and motor vehicles, which affect ambient air quality and human health (Kan et al., 2009, 2012; Liang et al., 2019). NO_X and SO_2 are two major gaseous pollutants that are essential precursors to secondary aerosol formation and acidification (Li et al., 2020). Therefore, the changes in NO_X and SO_2 emissions have been receiving increasing attention in China (Zhao et al., 2013; Zhao et al., 2018). To improve air quality, the Chinese government has promulgated a series of policies and regulations on SO_2 and NO_X control, especially since 2006 and 2011, respectively (Zheng et al., 2015).

Long-term observations of NO_X and SO_2 are not only critical for the integrated assessment of air quality and atmosphere–biosphere interactions (Swartz et al., 2020a), but also for the analysis of their reduction effects on $PM_{2.5}$, nitrate, sulphate, and near-surface O_3, providing a basis for further improvement of atmospheric protection policies (Yu et al., 2019). At a regional scale, long-term, reliable NO_X and SO_2 observations can also provide data to enable the scientific community to predict the future state of the atmosphere and assess environmental policies, serving to reduce environmental risks and enhance climate, weather, and air quality prediction capabilities (GAW, 2017). Numerous studies have evaluated the effectiveness of NO_X and SO_2 control in China from a long-term perspective by using emission inventories, satellite retrieval data, and ground monitoring data. For example, Sun et al. (2018) used a unified source emission inventory approach to quantify the historical emission trends of SO_2 and NO_X in China from 1949 to 2015; the results indicated that these pollutants reached an inflection point in 2006 and 2011, respectively. Source emission inventories by Kurokawa and Ohara (2020) revealed similar patterns. During the period from January 2005 to December 2015, the column concentration of NO_2 from ozone monitoring instrument (OMI) satellite retrieval indicated an increasing trend in most of China until a gradual or slight decrease in 2011 or 2012 (Cui et al., 2016). Zhao et al. (2019) used ground-based NO_2 observations to assess the effectiveness of pollution control policy in a southwestern city cluster and revealed fluctuations in NO_2 mixing ratios from 2008 to 2013, followed by an irregular declining trend after 2013. All these studies reported that NO_X and SO_2 mixing ratios have been effectively controlled in China despite the increasing economic development over the past decades.

The Yangtze River Delta (YRD) region is located in the central-eastern region of China, which has the largest economic output in China and has the sixth largest urban agglomeration in the world. The region covers an area of 359,100 km^2 and has a population of 224 million, accounting for 16.08 % of the country's population (Fang and Tian, 2020). Because of increases in population, urbanization, and industrialization in recent decades, the air pollution in the YRD has exhibited complex and regional characteristics (Li et al., 2019; Wang et al., 2019), and the YRD has become one of the most polluted regions in the

65 world (Xie, 2017b), with NO_X and SO_2 being the main factors that influence air quality in the region (Yang and Luo, 2019). Xu et al. (2008) compared observational data in 2005–2006 with those 10 years earlier and concluded that as early as the mid-1990s, SO_2 and NO_X mixing ratios had already become considerably high at the background station in the YRD; since then, anthropogenic emissions have caused a substantial increase in the NO_X concentration, making NO_X another major pollutant in addition to SO_2. The implementation of pollution control policies and continual innovation in SO_2 pollution control technology

70 have mitigated SO_2 pollution in the YRD, resulting in a consistent decrease in SO_2 mixing ratios (Qi et al., 2012); however, NO_X mixing ratios remain high (Shi et al., 2018).

In this paper, we present 11-year (2006–2016) surface NO_X and SO_2 observation data from Lin'an regional atmospheric background station. We analysed the long-term variations of NO_X and SO_2 and their influencing factors in the YRD background area to (1) assess the effectiveness of pollution control in the area and (2) provide a scientific basis and reference for future

75 pollution control strategies.

2   Information and methods

2.1 Site information

The Lin'an regional atmospheric background monitoring station (119°44′ E, 30°18′ N, 138.6 m a.s.l.; referred to LAN) is located in Lin'an District, Hangzhou City, Zhejiang Province (Fig. 1) and is one of the regional atmospheric background

80 stations operated by China Meteorological Administration; it is also a World Meteorological Organization (WMO) Global Atmospheric Watch (GAW) member station. LAN is located on an isolated hilltop, surrounded by hilly and mountainous terrain, with no large villages within a 3 km radius. It is within the region of subtropical monsoon climate, with the most dominant wind direction from the northeast and the secondary from the southwest. The seasonal variations in meteorological elements, namely atmospheric pressure (P), temperature (T), wind speed (WS), relative humidity (RH), and rose maps of wind

85 speed (WS) and wind direction frequency (WF), are presented in Fig. 2.

2.2 Observations and quality control methods

At the LAN station, observations of O_3, NO_X, SO_2, and CO are performed by an integrated observation and quality control system combining O_3, NO_X, SO_2, and CO analysers, calibration equipment, and ancillary materials, such as standard gases and zero air supply (Lin et al., 2009). NO_X and SO_2 were measured using a Model 42C-TL trace-level chemiluminescent analyser

90 and a Model 43C-TL trace-level pulsed fluorescence analyser (Thermo Fishier Scientific, MA, USA), respectively. In Model 42C-TL trace-level chemiluminescent analyser, NO_2 is converted to NO by a molybdenum NO_2-to-NO converter heated to about 325°C. The converter efficiency was checked annually using gas phase titration (GPT). If the converter efficiency is less than 96%, replace the converter. Data are recorded as 5 min averages. The meteorological parameters (WS, wind direction, T, and RH) for a given period were obtained from the routine meteorological observations at the station. The main objective of

operational observations of reactive gases at regional background stations is to obtain accurate trends in the measured reactive gases, for which reliable and comparable data are essential. Therefore, strict quality control measures were implemented during the observation process (Lin et al., 2019). The quality control measures mainly included the following: (1) daily zero and span checks (automatic); (2) monthly multi-point calibrations (≥5 points, including zero); (3) comparisons of reference SO_2/N_2 and NO/N_2 gas mixtures to the standards of the National Institute of Standards and Technology before and after their usage (periodically) to ensure data traceability; (4) instrument self-diagnosis, manual testing, checking, and maintenance (US EPA, 2017); and (5) data correction according to the quality control results, especially the results of zero/span checks and multipoint calibrations.

From 1 January 2006 to 31 December 2016, a total of 93,759 and 90,453 valid hourly average data points were obtained for NO_X and SO_2, respectively. Missing data totalled 2673 h and 5979 h for NO_X and SO_2, respectively. The missing NO_X data were mainly for the period from 2 to 13 February 2007 and from 24 July to 8 October 2012. The missing SO_2 data were mainly for the period from 23 September to 21 December 2013, from 8 to 26 May 2014, and from 17 October 2014 to 24 January 2015.

2.3 Data processing methods

(1) Data statistics. The daily means of NO_X and SO_2 were calculated using the hourly average data, and only daily mean data calculated from at least 18 hourly data were used as valid daily means. The monthly means of NO_X and SO_2 were calculated from the valid daily average data and considered valid if they were based on at least 21 valid daily averages (or at least 17 valid daily averages in February). Annual means were calculated on the basis of the complete monthly mean data each year. If a month's mean data were unavailable, we used an interpolating value from the corresponding monthly means in different years during the observation. In China, spring is from March to May, summer is from June to August, autumn is from September to November, and winter is from December to February.

(2) Monthly satellite based NO_2 OMI data were provided by Lin's research group at Peking University; the data were retrieved using an optimized inversion algorithm (Lin et al., 2014; Lin et al., 2015; Boersma et al., 2019). A grid range of 115.125° E–122.875° E and 27.125° N–35.875° N was selected to cover the entire YRD region.

2.4 Concentration weighted trajectory method

We used the concentration weighted trajectory (CWT) method to identify potential source areas (PSAs) of NO_X and SO_2 because this method can effectively distinguish the relative strength of potential sources (Xin et al., 2016). In the CWT method, the study area is divided into $i \times j$ small grids with equal size, and each grid (i, j) is assigned a weighted concentration according to the following equation:

$$C_{ij} = \frac{1}{\sum_{k=1}^{m} \tau_{ijk}} \sum_{k=1}^{m} C_k \, \tau_{ijk} \qquad (1)$$

Where k denotes the indicator of a trajectory, m denotes the total number of trajectories, C_k denotes the concentration observed when trajectory k arrives, and τ_{ijk} is the residence time of trajectory k in the ij_{th} grid cell. To reduce errors in the more distant grids, an empirical weighting factor W_{ij} is introduced (Wang et al., 2006; Deng et al., 2020), with the following equation:

$$\text{CWT(i,j)} = W_{ij} \times C_{ij} \qquad (2)$$

$$W_{ij} = \begin{cases} 1 & (n_{i,j} > 3n_{ave}) \\ 0.7 & (3n_{ave} < n_{i,j} < 1.5n_{ave}) \\ 0.42 & (1.5n_{ave} < n_{i,j} < n_{ave}) \\ 0.05 & (n_{i,j} < n_{ave}) \end{cases} \qquad (3)$$

Here,

$$n_{ave} = \frac{D \times t \times n}{i \times j} \qquad (4)$$

Where D denotes the number of days included, t denotes the number of trajectories per day, n denotes the trajectory endpoints of each trajectory, and $i \times j$ denotes the total number of grids.

We used a hybrid single-particle Lagrangian integrated trajectory model (Hysplit4.9) from National Oceanic and Atmospheric Administration, USA, to calculate the 24-h backward trajectories at 10 m above ground level over LAN during 2006–2016; the NCEP–NCAR reanalysis meteorological data set (https://ready.arl.noaa.gov/archives.php) and was used to calculate the trajectories and atmospheric mixed layer heights. The computed backward trajectories were subsequently processed using the TrajSat plug-in for CWT in Meteoinfo software (Wang, 2014), covering the region located within 20–40° N and 110–130° E and with a grid size resolution of 0.5 ° × 0.5 °.

3 Results and discussion

3.1 Observational levels and comparison with other sites

The hourly average SO_2 mixing ratios ranged from 0.1 ppb to 128.6 ppb, which were all below the GB3095–2012 secondary standard limit for SO_2 (190 ppb). The hourly average NO_X mixing ratios at LAN ranged from 0.4 ppb to 165.6 ppb, with NO_2 mixing ratios ranging from 0.2 ppb to 106.8 ppb. Only 3 hours' data exceeded the secondary standard limit value for NO_2 (106 ppb) as stated in the national ambient air quality standard (GB3095–2012). It should be mentioned that the measurements of NO_2 was converted to NO by a molybdenum NO_2-to-NO converter heated to about 325 °C, which suffered from the interference of other NO_y compounds such as PAN and HNO_3 (Steinbacher et al., 2007; Jung et al., 2017). This implies that the measured NO_2 concentrations have to be viewed as an upper limit. However, it is not possible to quantify the overestimation due to the lack of other information. The interference might be enhanced with the increasing PAN/NOx ratios. Qiu et al. (2020)

5

Table 1 presents annual statistics of the NO$_2$, NO$_X$ and SO$_2$ mixing ratios observed at LAN between 2006 and 2016. The overall average mixing ratios with ± 1 standard deviation of for NO$_X$ (NO$_2$) and SO$_2$ from 2006 to 2016 were 13.6 ± 1.2 ppb (12.5±4.6 ppb) and 7.0 ± 4.2 ppb, respectively, with the highest NO$_x$ (NO$_2$) value being observed in 2012 and the highest SO$_2$ in 2006. NO$_2$ was the dominant form of NO$_X$, accounting for 82.2 % of NO$_X$ (according to the slope value from the reduced major axis regression on hourly average NO$_2$ and NO$_X$ data). The average NO$_2$ mixing ratio was 12.5 ± 4.6 ppb, which was below the primary annual limit of 21.2 ppb in GB 3095–2012. Some information on NO$_2$(NO) can be seen the supplementary material (Tab.S1). The average SO$_2$ mixing ratio from 2006 to 2016 is close to the primary annual limit of 7.6 ppb in GB3095–2012. However, the annual average SO$_2$ mixing ratios (10.6–14.6 ppb) from 2006 to 2008 was much higher than the limit of the primary standard though lower than the limit of the secondary standard (22.8 ppb).

Table 2 compares the levels of NO$_X$ and SO$_2$ mixing ratios at LAN with those corresponding SO$_2$/NO$_X$ ratios at other background stations in seven geographic regions of China: north, east, south, northeast, northwest, southwest, and central China. The NO$_X$ mixing ratio at LAN was slightly higher than that at Shangdianzi (12.7 ± 11.8 ppb) in northern China, equal to that at Dinghushan (13.6 ppb) in southern China, and much higher than those at Wuyishan (2.70 ppb) in eastern China, Fukang (8.3 ppb) in northwest China, Changbai Mountain (4.7 ppb) in northeast China, Jinsha (5.6 ± 5.5 ppb) in central China, and Southwest Gongga Mountain (0.90 ppb). These results indicate that LAN recorded the highest level of NO$_X$ among the regional atmospheric background stations in China, which could be attributed to the developed economy of the YRD region. The SO$_2$ mixing ratio at LAN was close to that at Shangdianzi (7.6 ± 10.2 ppb) in northern China, higher than that at Dinghu Mountain (6.5 ppb) in southern China, and much higher than those at Wuyishan (1.48 ppb) in eastern China, Changbai Mountain (2.1 ppb) in northeast China, Fukang (2.2 ppb) in northwest China, Gongga Mountain (0.19 ppb), and Jinsha (2.8 ± 5.5 ppb) in central China. The regional difference in NO$_X$ and SO$_2$ was closely related to the diverse levels of economic development in China's regions because it was broadly characterised by a higher level in the eastern than in central and western regions. The SO$_2$/NO$_X$ ratio at LAN was at a high level in China, which reflects the different energy structures to some extent.

3.2 Seasonal variations

Figure 3 illustrates the average seasonal variations in NO$_X$ and SO$_2$ mixing ratios at LAN. The maximum monthly average mixing ratios of NO$_X$ and SO$_2$ were observed in December and January, at 23.5 ± 4.4 ppb and 11.9 ± 6.2 ppb, respectively. The minimum values both occurred in July, at 7.1 ± 0.8 ppb and 2.8 ± 2.3 ppb, respectively. The average monthly variations in NO$_X$ exhibited significant correlations with the monthly NO$_2$ satellite data ($R^2 = 0.82$, $P < 0.001$). Seasonal variation patterns of NO$_X$ and SO$_2$ look alike, showing a concave shape with its minimum in summer. The highest mixing ratios occurred in

winter (NO$_X$: 19.5 ppb; SO$_2$: 10.1 ppb), followed by spring (NO$_X$: 13.4 ppb; SO$_2$: 7.8 ppb), autumn (NO$_X$: 13.6 ppb; SO$_2$: 6.7 ppb), and summer (NO$_X$: 8.1 ppb; SO$_2$: 3.3 ppb). The monthly average mixing ratios of both NO$_X$ and SO$_2$ showed a dip in February—a phenomenon also observed in NO$_X$ and SO$_2$ (Wang et al., 2016; Xue et al., 2020) and NO$_3^-$ and SO$_4^{2-}$ in PM$_{2.5}$ in Shanghai (Duan et al., 2020). The source emission inventory data indicated that NO$_X$ and SO$_2$ emissions from industry, transportation, and coal-fired power plants were all lower in February than in January and March throughout China (Li et al., 2017), which may be related to decreased emissions due to lower economic activity during Chinese Spring Festival. In addition, the higher RH in February (Fig. 2) might have led to higher NO$_X$ and SO$_2$ removal rates.

3.3 Diurnal variations

Figure 4 shows the annual and seasonal average diurnal variations in NO$_X$ and SO$_2$ at LAN from 2006 to 2016, along with the annual average diurnal variations in NO$_X$ and SO$_2$ at some other sites in the YRD. The overall diurnal profile of NO$_X$ displayed a double-peak and double-valley pattern (Fig. 4a). The valley values occurred at 05:00–06:00 and 13:00, with mixing ratios of 12.3 ppb and 10.0 ppb, respectively, and the peak values occurred at 09:00 and 19:00, with mixing ratios of 13.1 ppb and 14.4 ppb, respectively. Surrounding areas, such as Chongming, Pudong (Xue et al., 2020), and Xujiahui (Gao et al., 2017) in Shanghai City, Hangzhou (Zhou et al., 2020) in Zhejiang Province, and Nanjing (Wang et al., 2017) in Jiangsu Province also exhibited a double-peak and double-valley type of average diurnal variation in NOx (Fig. 4a), indicating a regional NO$_X$ pollution characteristic. However, at most atmospheric background stations, the average diurnal variations in NO$_X$ exhibited a single-peaked and single-valley pattern, such as those at Xinglong in north China (Yang et al., 2012), Tianhu in the Pearl River Delta (Shen et al., 2019), Dae Hung in South Korea (Pandey et al., 2008), and Mount Cimone in Italy (Cristofanelli et al., 2016), suggesting a more complex anthropogenic influence in the YRD region. In summer, the seasonal average diurnal variation in NO$_X$ showed a morning peak at 08:00, which time is 1 to 2 h earlier than that occurred in other seasons (Fig. 4c). SO$_2$ at LAN showed relatively small average diurnal variation (Fig. 4b), with higher mixing ratios from midnight to noontime and lower ones during later afternoon and evening. The average diurnal amplitude of SO$_2$ at LAN was much smaller than those found in Nanjing and Jiaxing. The seasonal average diurnal profiles of SO$_2$ at LAN were similar to the annual average one except for that in winter, which had a peak around noon (Fig. 4d).

The diurnal variation of pollutants emitted at ground level are closely related to the intensity of emissions, atmospheric transport, diurnal development in boundary layer height, and atmospheric photochemical reactions (Resmi et al., 2020). The mixing layer depth (MLD) was much lower at night than during the daytime, as shown in Fig. 4b. Low MLDs at night are not conducive to pollutant dispersion, whereas high MLDs during the daytime are conducive to pollutant dispersion. This day-night difference in the MLD is one of the factors causing lower levels of SO$_2$ and NO$_X$ during afternoon hours. Photochemistry during the daytime also contributes to rapid chemical transformation of SO$_2$ and NO$_X$, which results in low NO$_X$ and SO$_2$ mixing ratios in the afternoon. Overall, the morning peak of NO$_X$ was lower than the evening peak, the morning peak of SO$_2$ was higher than the evening subpeak, and the morning peak of SO$_2$ was not as protruding as and occurred slightly later than that of NO$_X$, reflecting the differences in their sources. The morning peak of NO$_X$ may be influenced by vehicle emissions

7

during the morning rush hour, and the early peak of SO_2 may be more influenced by vertical changes during the developing mixed layer depth height (Qi et al., 2012). The evening peaks of NO_X and SO_2 were relatively similar because both were closely related to the MLD decrease and for NO_X likely also vehicle emissions during the evening rush hour.

3.4 Influence of meteorological factors

Changes in meteorological factors have considerable effects on the levels of air pollutants. In this section, we investigate the influences of meteorological factors on the variations in NO_X and SO_2 mixing ratios through statistical plots showing relationships between pollutant concentrations and meteorological factors as well as correlation analysis. The variation characteristics of hourly average mixing ratios of NO_X and SO_2 along with meteorological parameters are presented in Fig. 5. The data are grouped into three subsets corresponding to time periods: I (2006–2009), II (2010–2013) and III (2014–2016). The variation characteristics of NO_X and SO_2 with WS (Fig. 5a,b) were consistent during period I, showing decreases of NO_X and SO_2 with increasing WS. Higher WS facilitated the dilution of NO_X and SO_2 and vice versa. However, the situation for SO_2 was different during period II and III, when the SO_2 level was stable with the change of WS. The correlation of T between the two pollutants varied considerably, with the SO_2 mixing ratios decreasing nearly monotonically with increasing T (Fig. 5d), whereas NO_X increased with increasing T in the low temperature range and decreased with increasing T in the high temperature range (Fig. 5c). Fig. 5c indicates a positive correlation between NO_X and T in winter and negative correlations in other seasons, but the positive correlation in winter is weak and insignificant (Table 3). Pandey et al. (2008) reported that low T might facilitate the increase of NO_X emissions from motor vehicle exhaust. The variations in NO_X and SO_2 with RH (Fig. 5e,f) exhibit a convex pattern and the former patterns in 3 different periods are well consistent but the latter ones are not at low RH. The correlation between SO_2 and RH was stronger than that of NO_X and RH (Table 3). The variation characteristics of NO_X and SO_2 mixing ratios with the MLD exhibited diverse patterns (Fig. 5g,h). The mixing ratio of NO_X decreased with increasing MLD. However, the SO_2 levels during period II and III remained nearly stable in the whole MLD range and a slight decline of SO_2 with increasing MLD was only observed during period I. The difference in NO_X and SO_2 mixing ratios with the MLD implies that the NO_X sources mostly impacting the LAN site should be mainly in the near-surface layer, such as emissions from motor vehicles and small burners, whereas SO_2 may originate from the vertical exchange of elevated sources transported in the higher altitude layer (200–1300 m).

Figure 6 displays the rose diagrams of NO_X and SO_2 mixing ratios in different seasons. There are some seasonal differences in the dependence of NO_X and SO_2 on wind direction. In summer, the high mixing ratios of NO_X and SO_2 were mainly from the NW–NNE and SSW–NW sectors, respectively (Fig. 6b). In other seasons, relatively high NO_X and SO_2 values were mainly from the N–ENE and S–WSW directions, respectively, under the influences of the dominant and subdominant WDs (Fig. 2b, d). Overall, NO_X and SO_2 observed at LAN originated mainly from the NW-ENE and SSW-NW sectors, respectively. However, this result provides only little information about the actual geographic distributions of major NO_X and SO_2 sources influencing LAN. Therefore, we used the CWT method to identify the PSAs for NO_X and SO_2. Fig. 7 presents the areas, from which NO_X and SO_2 observed at LAN originated. Although the PSAs covered the entire YRD, the PSAs for the highest NO_X and SO_2

levels appeared mainly in the eastern coastal region, which is closely related to the booming local economy. More obvious provincial differences were observed in a higher PSA for NO_X than that for SO_2. Temporally, the high PSA (>10 ppb) of NO_X and SO_2 was most extensive in winter, followed by spring and autumn, with the least extensive PSA in summer. The NO_X PSAs over coastal areas were more extensive than those for SO_2 in each season. The YRD is one of the five major port clusters in China; thus, this region's ship emissions might be a major cause of this difference (Fan et al., 2016; Wan et al., 2020). The CWT analysis indicated that SO_2 was mainly influenced by industrial emissions from inland areas, whereas NO_X was mainly influenced by both inland and marine traffic.

3.5 Long-term variations in NOx and SO₂ mixing ratios

Fig. 8 displays the variations in the annual and seasonal average NO_X and SO_2 mixing ratios observed at LAN during 2006–2016, together with estimated annual emissions in the YRD. The annual average of NO_X showed an increase followed by a decrease, while that of SO_2 experienced a nearly monotonic decrease. The annual NO_X mixing ratio revealed an increase, with a rate of +0.31 ppb/yr ($R^2 = 0.28$, $P = 0.16$) during 2006–2011 and a significant decreasing trend, with a rate of −0.78 ppb/yr or −5.16 %/yr ($R^2 = 0.85$, $P < 0.01$) during 2011–2016 (Fig. 8a). The decreasing rate was less than that found in urban Shanghai (-2.1 ppb/yr; Gao et al., 2017). Selecting 2006 as the base year, we compared the annual percentage change in NO_X at LAN (-0.49 %/yr) during 2006–2016 with those of other regions over the same period. The *Ecological and Environmental Status Bulletin* (Shanghai Municipal Bureau of Ecology and Environment, 2007–2017; Department of Ecology and Environment of Zhejiang Province, 2007–2017; Department of Ecology and Environment of Jiangsu Province, 2007–2017) reported a similar change of −0.45 %/yr in the YRD region (without data for Anhui Province), reflecting the suitable regional representativeness of LAN. The annual percentage decrease of NO_X at LAN and in the YRD was much smaller than those in many regions—for example, the Pearl River Delta in China (−2.84 %/yr; Yan et al., 2020), Kraków City in Poland (−2.21%/yr; Agnieszka and Gruszecka-Kosowska, 2020), at Preila station in Lithuania (−1.60 %/yr; Davuliene et al., 2021), and in New York City in the United States (−3.46 %/yr; Squizzato et al., 2018)—but more favourable than those in some other regions, such as Wuhan City in China (+2.08 %/yr; Li et al., 2020) and Amersfoort City (+6.50 %/yr) and Louis Trichardt City in South Africa (+1.85 %/yr; Swartz et al., 2020b). Compared with other background regions in China, the annual change of NO_X at LAN was less favourable than that in north China (−3.34 %/yr) with a base year of 2005 (Bai et al., 2015) and more favourable than that in northwest China (+12.98 %/yr) with a base year of 2010 (Li et al., 2019).

Figure 8 also presents the NOx emission data from the *China Ecological Environment Bulletin* in different years. The change of the annual average NOx mixing ratio was highly correlated with the total NO_X emissions ($R^2 = 0.92$, $P < 0.001$) and total industrial emissions ($R^2 = 0.94$, $P < 0.001$) in the YRD region. The peak surface NO_X mixing ratio was observed in 2011. Since China began to control and reduce NO_X emissions as part of the *12th Five-Year Plan* (2011–2015) and promulgated the strict *Air Pollution Prevention and Control Action Plan* in 2013, many flue gas denitrification systems have been installed in coal-fired power plants and heavy industry operations (Zhao et al., 2019), resulting in a decrease in annual NO_X emission since 2011. As seen in Figure 8a, the total and the industrial NOx emission showed increasing trends with 5.84 %/yr ($R^2 = 0.91$, $P =$

285 ($R^2 = 0.84$, $P = 0.011$), respectively, from 2011-2016. The seasonal long-term trends of NO_X did always resemble the annual

trend. While seasonal NO_X mixing ratios in winter, autumn, and spring increased before 2011 and then decreased, just like the

annual NO_X mixing ratio did, the seasonal NO_X mixing ratio in summer exhibited a nearly monotonic decreases from 2006 to

2016 at 0.11 ppb/yr ($R^2 = 0.20$, $P = 0.09$) (Fig. 8c). Regarding the seasonal linear fitting trends, the highest increasing and

declining trends were observed in winter (+1.29 ppb/ yr, $R^2 = 0.52$, $P = 0.06$; −2.33 ppb/yr, $R^2 = 0.94$, $P < 0.01$), followed by

290 autumn (+1.24 ppb/yr, $R^2 = 0.65$, $P = 0.02$; −0.41 ppb/yr, $R^2 = 0.12$, $P = 0.30$) and spring (+0.31 ppb/yr, $R^2 = 0.93$, $P < 0.001$;

−1.16 ppb/yr, $R^2 = 0.76$, $P = 0.09$). We found a significant correlation ($P < 0.05$) between surface NO_2 mixing ratio and OMI

NO_2 vertical column density over YRD (Fig. S3b). To better compare the changes in the two over the same period, we have

fitted a linear fit to the data from 2006 to 2011 and from 2011 to 2016 respectively (Fig.S3a). The surface and the OMI NO_2

increased at 2.23%/yr ($R^2 = 0.264$, $P = 0.17$) and 5.87%/yr ($R^2 = 0.855$, $P < 0.01$) (based on 2006), respectively, during the up

295 period and decreased at −4.98%/yr ($R^2 = 0.823$, $P < 0.01$) and −4.22%/yr ($R^2 = 0.897$, $P < 0.01$), respectively, during the

declining period.

Annual mean SO_2 mixing ratios revealed a significant decreasing trend (−0.99 ppb/yr, $R^2 = 0.92$, $P < 0.001$) during 2006-2016

(Fig. 8b). The annual decreasing rate of SO_2 at LAN (−8.27 %/yr) was more rapid than those in the whole YRD (−6.65 %/yr),

in the background area in north China (−0.78 %/yr; Bai et al., 2015), and in northwest China (−5.4 %/yr; Li et al., 2019).

300 Different from NO_X, the annual average of SO_2 at LAN decreased more rapidly than in most of the aforementioned regions

(Table 4), which demonstrates the effectiveness of the policies in controlling SO_2 emission during the observation period in

the YRD.

The change in the annual SO_2 mixing ratio was closely correlated with changes in thermal power plants SO_2 industrial emission

($R^2 = 0.89$, $P < 0.001$), industrial SO_2 emission ($R^2 = 0.76$, $P < 0.001$) and total SO_2 emission ($R^2 = 0.78$, $P < 0.001$) in the

305 YRD (Fig. 8b). In 2011, the SO_2 mixing ratio rebounded slightly, with an increase of 9 % compared with the value in 2010.

This seemed to be consistent with the variation of industrial SO_2 emission. The weakening impact of the global financial crisis

and the recovery of industry in the YRD region may explain this slight rebound in SO_2 emissions (Xie, 2017b). Seasonally,

the SO_2 mixing ratio exhibited the strongest decreasing trend (−1.69 ppb/yr, $R^2 = 0.90$, $P < 0.001$) in winter, followed by spring

(−1.05 ppb/yr, $R^2 = 0.97$, $P < 0.001$) and autumn (−0.99 ppb/yr, $R^2 = 0.93$, $P < 0.001$), with the smallest decreasing trend

310 observed in summer (−0.35 ppb/yr, $R^2 = 0.61$, $P < 0.001$).

In the annual statistics, the 95th and 5th percentile of the pollutants' concentrations can be regarded as influenced by polluted

and clean air masses, respectively. The annual trends of the 95th percentile of NO_X and SO_2 (Fig. 9a) exhibited similar patterns

to the corresponding trends in annual average mixing ratios (Fig. 8a, b), but the peak of the 95th percentile of NO_X occurred

in 2012, instead of in 2011. Hao and Song (2018) noted that the NO_X emissions from vehicles peaked in Hangzhou and Ningbo

315 in 2012, which may explain the peak of the 95th percentile occurring later than that in the annual data. Moreover, the 95th

percentile of the SO_2 mixing ratio decreased at a remarkable rate (−8.9 ppb/yr) from 2007 to 2009, which is approximately 2.8

times as strong as the overall rate of decrease during the 11-year period (−3.2 ppb/yr). Substantial decreases were also found

in the 95th percentiles of the CO mixing ratio (Chen et al., 2020) and the NO_X mixing ratio from 2007 to 2009 at LAN. It is highly possible that this phenomenon was caused by reduced industrial productions and related emissions following the 2008 global financial crisis. As displayed in Fig. 9b, the level of NO_X in cleaner air mass arriving at LAN exhibited an increasing trend, with a rate of +0.17 ppb/yr, from 2006 to 2014 ($R^2 = 0.86$, $P < 0.001$) and then declined after 2014. This is inconsistent with the trend of the 95th percentile of the NO_x mixing ratio, suggesting the polluted and relative clean air masses arriving at LAN were impacted by different emission sources of NO_x. Interestingly, the 5th percentile of the NO_x level was significantly correlated ($R^2 = 0.74$, $P < 0.001$) with the road emissions of NO_2 in the YRD (Kurokawa and Ohara, 2020), suggesting that the lower end of NO_x mixing ratios was mainly determined by long-range transported background air containing NO_x from road emissions, while the high end was mainly associated with emissions from industrial production as well as power generation. The level of SO_2 in cleaner air mass exhibited a decreasing trend at a rate of −0.2 ppb/yr ($R^2 = 0.61$, $P < 0.01$).

Figure 10 displays the scatter plot of the daily average SO_2 and NO_X mixing ratio during period I, II and III at LAN. Reduced major axis regressions were performed on three data subsets. The daily mean mixing ratios of NO_X were significantly ($R^2 = 0.29$, $P < 0.001$) and positively correlated with those of SO_2. The ratios of SO_2 to NO_X (SO_2/NO_X) were 0.96, 0.53, and 0.33 (slopes in the regression lines) during period I, II and III, respectively. The decreasing SO_2/NO_X suggests that SO_2 emissions were more efficiently reduced than NO_X emissions. Such a change in emission ratio not only affected ambient SO_2/NO_X but also the ratios of sulphate/nitrate in $PM_{2.5}$ in Shanghai from 2009 to 2012 (Zhao et al., 2015) SO_4^{2-}/NO_3^- in rainwater in Hangzhou (Yang, 2018; Xu et al., 2019). These results indicate that NO_X has been gaining a more important role in the processes of precipitation acidification and secondary inorganic aerosol formation in the YRD region. Therefore, NO_X emission reduction should be further strengthened in subsequent air pollution control measures and legislation in the YRD region.

Figure 11 reveals the average diurnal variations in NO_X and SO_2 during the period I, II and III. During these three periods, the average diurnal curves in NO_X exhibited a valley around 13:00, with minimum values of 7.5 ppb, 11.2ppb, and 9.2 ppb, respectively. The morning and evening NO_X peaks, which occurred respectively at 09:00 and 19:00, became increasingly distinct over time (Fig. 11a, c, e). The morning and evening peak NO_X values were 9.8 ppb and 10.9 ppb during period I, 14.6 ppb and 15.8 ppb during period II, and 12.3 ppb and 13.6 ppb during period III. The gradual protruding of the morning and evening peaks should be mainly caused by increasing vehicle emissions during the morning and evening rush hours. According to the 2010 Annual Report on China's Motor Vehicle Pollution Prevention and Control, the state introduced a series of policies to promote automobile and motorbike ownership in response to the international financial crisis and to ensure economic growth; these policies effectively stimulated the automobile market (Mi and Qin, 2011; Hao and Song, 2018) and led to an increase in vehicle emissions and atmospheric oxidation in the YRD region (Yu et al., 2019). Thus, the NO_X mixing ratios around the morning and evening peaks were much higher than those at night during period II (Fig. 11e), which differs much from the pattern during period I (Fig. 11a). The disappearance of the small peak around 01:00 at night during 2012–2016 may be related to the introduction of stricter air pollution control policies for factories that emit at night. Small peaks in NO_X and SO_2 occurred between 01:00 and 02:00, which might be related to nighttime emissions from unscrupulous enterprises (Fan et al., 2013) or

more production activities with lower electricity prices after midnight in response to the financial pressure of the 2008 economic crisis and the corresponding increase in electricity prices for industrial users (Sun, 2008). In spite of these two reasons, however, it's really hard to tell exactly why these small peaks dominate after midnight.

355   The average diurnal variation curve of SO_2 at LAN period I (Fig. 11b) is of the single-valley type, with an average valley mixing ratio of 6.5 ppb. After 2010, the peak shape has changed from single-valley type to the double-peak and double-valley type (Fig. 11d, f). The valleys of SO_2 during period II occurred at 06:00 and 15:00, with average mixing ratios of 5.2 ppb and 4.7 ppb, and the peaks occurred at 10:00 and 19:00, with average mixing ratios of 5.9 ppb and 5.3 ppb, respectively. The NO_X and SO_2 evening peaks occurred at the same time (19:00), but the SO_2 morning peak time was 1 hour later than the NO_X

360   morning peak (09:00), indicating that the NO_X and SO_2 morning peaks were influenced by different sources, whereas the evening peaks were from similar sources. The formation of the SO_2 morning peak may be mainly related to the vertical exchange during the development of the atmospheric boundary layer and the air in the upper layer with a higher SO_2 mixing ratio than that at the surface draining down. The formation of the evening peaks of NO_X and SO_2 may be mainly related to the increase in motor vehicle and residential sources emissions, which are stronger in the rush and cooking hours and that of SO_2

365   may be probably more due to the reduction of power plants emissions. Compared with that during period II, the SO_2 mixing ratios at the morning and evening peaks in period III were approximately 3 ppb lower, suggesting that the large emitters that release SO_2 all the time were emitting less and less.

Conclusions

In this study, we characterized the seasonal and diurnal variations and analysed the long-term trends in NO_X and SO_2 mixing

370   ratios in the YRD background area during the period of 2006–2016. We also tried to understand the variations and trends in terms of the changes in emissions and meteorological conditions. The hourly average mixing ratios of NO_X (NO_2) and SO_2 at the LAN background station varied in the ranges of 0.4–165.6 ppb (0.2–106.8 ppb) and 0.1–128.6 ppb, respectively. The levels of NO_X and SO_2 were highest in winter, followed by spring and autumn, and lowest in summer. Although a significant correlation was observed between the daily average mixing ratios of NO_X and SO_2 ($R^2 = 0.29$, $P < 0.001$), their average diurnal

375   variation characteristics differed from each other, with morning peaks in SO_2 occurring later than in NO_X.

The annual average mixing ratio of NO_X (NO_2) fluctuated upwards between 2006 and 2011 (+0.31 ppb/yr, $P = 0.16$) (+0.27 ppb/yr, $P = 0.17$) with a mean value of 13.8 ppb and then began to decrease significantly from 2011 to 2016 (–0.78 ppb/yr, $P < 0.01$) (–0.70 ppb/yr, $P < 0.01$), with a mean value of 13.7 ppb (12.5 ppb). The annual average mixing ratio of NO_X was significantly correlated with the industrial ($R^2 = 0.81$, $P < 0.001$, 2006–2016) and total ($R^2 = 0.88$, $P < 0.001$, 2006–2016) NO_X

380   emissions in the YRD, so as between surface and OMI NO_2 (Fig.S3b, $R^2 = 0.61$, $P < 0.01$). The annual 95 % percentile of NO_X mixing ratios followed a similar trend to the annual average, whereas the 5th percentile levels fluctuated upwards at +0.17 ppb/yr from 2006 to 2014, reflecting the increasing regional background level of NO_X in the YRD during those years, which was related to the continued increase in vehicle numbers in the YRD. The annual average mixing ratio of SO_2 exhibited a rapid

and significant decreasing trend (–0.99 ppb/yr, $P < 0.001$) and was closely correlated to total SO_2 emission ($R^2 = 0.78$, $P <$ 0.001) , total SO_2 industrial emission ($R^2 = 0.76$, $P < 0.001$) and total thermal power plants SO_2 industrial emission ($R^2 = 0.89$, $P < 0.001$) in the YRD. The reduced emissions were resulted from the strong and effective introduction of national control policies. The yearly decrease of SO_2/NO_X. ratios suggest a more effective reduction in SO_2 than in NO_X. Thus, NO_X emission control needs to be further strengthened in the future.

We found gradual changes in diurnal patterns of both gases. After 2010, both NO_X and SO_2 showed diurnal patterns with two peaks and two valleys. The morning peak of NO_X occurred at approximately 09:00, earlier than that of SO_2 (10:00), and the evening peak occurred at the same time as SO_2 (19:00). The morning and evening peaks of both gases protruded gradually. This phenomenon can hardly be attributed to changes in meteorological conditions (such as the MLD). We believe that changes in major sources of NO_X and SO_2 should be the cause, with increasing NO_X emission from vehicles resulting in higher NO_X peaks during rush hours and reduced SO_2 emissions from power plants and other large point sources making the SO_2 peaks relatively protruding.

Data availability. The data of stationary measurements are available upon request to the contact author Weili Lin (linwl@muc.edu.cn).

Author contributions. QY wrote the paper, WL and XX developed the idea f, formulated the research goals, and edit the paper. QM and JY carried out the measurement of NO_X and SO_2 and analysed the meteorological data.

Competing interests. The authors declare that they have no conflict of interest.

Acknowledgements.

References

Agnieszka, P. T., and Gruszecka-Kosowska: The Condition of Air Pollution in Kraków, Poland, in 2005–2020, with Health Risk Assessment, Int. J. Env. Res. Pub. He., 17, E6063, https://doi.org/10.3390/ijerph17176063, 2020.

Bai, J., Wu, J., Chai, W., Wang, P., and Wang, G.: Long-Term Variation of Trace Gases and Particulate Matter at an Atmospheric Background Station in North China, Forn.Earth Sci., 248–263, https://doi.org/10.12677/ag.2015.53025, 2015.

Chen, L.: Measure and Study on the Atmospheric Pollutants in Three Typical Regional Background Stations of China, Lanzhou University, 2012.

Chen, Y., Ma, Q., Lin, W., Xu, X., Yao, J., and Gao, W.: Measurement report: Long-term variations in carbon monoxide at a background station in China's Yangtze River Delta region, Atmos. Chem. Phys., 20, 15969–15982, https://doi.org/10.5194/acp-20-15969-2020, 2020.

Cheng, L., Ji, D., He, J., Li, L., Du, L., Cui, Y., Zhang, H., Zhou, L., Li, Z., and Zhou, Y.: Characteristics of air pollutants and greenhouse gases at a regional background station in Southwestern China, Aerosol. Air. Qual. Res, 19, 1007–1023, https://doi.org/10.4209/aaqr.2018.11.0397, 2019.

Cristofanelli, P., Landi, T. C., Calzolari, F., Duchi, R., Marinoni, A., Rinaldi, M., and Bonasoni, P.: Summer atmospheric composition over the Mediterranean basin: Investigation on transport processes and pollutant export to the free troposphere by observations at the WMO/GAW Mt. Cimone global station (Italy, 2165 m a.s.l.), Atmos. Env., 141, 139–152, https://doi.org/10.1016/j.atmosenv.2016.06.048, 2016.

Cui, Y., Lin, J., Song, C., Liu, M., Yan, Y., Xu, Y., and Huang, B.: Rapid growth in nitrogen dioxide pollution over Western China, 2005–2013, Atmos. Chem. Phys., 16, 6207–6221, https://doi.org/10.5194/acp-16-6207-2016, 2016.

Davuliene, L., Jasineviciene, D., Garbariene, I., Andriejauskiene, J., Ulevicius, V., and Bycenkiene, S.: Long-term air pollution trend analysis in the South-eastern Baltic region, 1981–2017, Atmos. Res., 247, 105191, https://doi.org/10.1016/j.atmosres.2020.105191, 2021.

Deng, J., Guo, H., Zhang, H., Zhu, J., Wang, X. and Fu, P.: Source apportionment of black carbon aerosols from light absorption observation and source-oriented modeling: an implication in a coastal city in China, Atmos. Chem. Phys., 20, 14419–14435, https://doi.org/10.5194/acp-20-14419-2020, 2020.

Duan, L., Yan, L., and Xiu, G.: Online Measurement of $PM_{2.5}$ at an Air Monitoring Supersite in Yangtze River Delta: Temporal Variation and Source Identification, Atmosphere, 11, 789, https://doi.org/10.3390/atmos11080789, 2020.

Fan, Q., Zhang, Y., Ma, W., Ma, H., Feng, J., Yu, Q., Yang, X., Ng, S. K. W., Fu, Q., and Chen, L.: Spatial and Seasonal Dynamics of Ship Emissions over the Yangtze River Delta and East China Sea and Their Potential Environmental Influence, Env. Sci. Technol., 50, 1322–1329, https://doi.org/10.1021/acs.est.5b03965, 2016.

Fang, G. W., Qingling, and Tian, L.: Green development of Yangtze River Delta in China under Population-Resources-Environment-Development-Satisfaction perspective, Sci. Tot. Env., 727, https://doi.org/10.1016/j.scitotenv.2020.138710, 2020.

Gao, W., Tie, X., Xu, J., Huang, R., Mao, X., and Zhou, G. C., Luyu Long-term trend of O_3 in a mega City (Shanghai), China: Characteristics, causes, and interactions with precursors, Sci. Tot. Env., 603–604, 425–433, https://doi.org/10.1016/j.scitotenv.2017.06.099, 2017.

Ge, Y.F., Shi, X.W., Ma, Y., Zhang, W.Q., Ren, X.R., Zheng, J., Zhang, Y.C.: Seasonality of nitrous acid near an industry zone in the Yangtze River Delta region of China: Formation mechanisms and contribution to the atmospheric oxidation capacity, Atmos. Environ., 254, 118420, https://doi.org/10.1016/j.atmosenv.2021.118420, 2021.

Hao, Y., and Song, X.: Research on trends and spatial distribution of vehicular emissions and its control measure assessment in the Yangtze River Delta, China, for 1999–2015, Env. Sci. Pollut. R., 25, 36503–36517, https://doi.org/10.1007/s11356-018-3476-y, 2018.

Jia, S.H., Simultaneous observation and analysis of O3 and PAN in North China, Ph.D. thesis, Chinese Academy of Meteorological Sciences, China, 93 pp., 2015.

Jia, C.H., Tong, S.R., Zhang, W.Q., Zhang, X.R., Li, W.R., Wang, Z., Wang, L. L., Liu, Z.R., Hu, B., Zhao, P.S., Ge, M.F.: Pollution characteristics and potential sources of nitrous acid (HONO) in early autumn 2018 of Beijing, Sci. Total Environ., 735, 139317, https://doi.org/10.1016/j.scitotenv.2020.139317, 2020.

Jung, J., Lee, J., Kim, B., and Oh, S.: Seasonal variations in the NO2 artifact from chemiluminescence measurements with a molybdenum converter at a suburban site in Korea (downwind of the Asian continental outflow) during 2015–2016, Atmos. Environ., 165, 290-300, https://doi.org/10.1016/j.atmosenv.2017.07.010, 2017.

Kan, H., Chen, B., and Hong, C.: Health Impact of Outdoor Air Pollution in China: Current Knowledge and Future Research Needs, Environ. Health. Persp., 117, A187, https://doi.org/10.1289/ehp.12737, 2009.

14

Kan, H., Chen, R., and Tong, S.: Ambient air pollution, climate change, and population health in China, Environ. Int., 42, 10–19, https://doi.org/10.1016/j.envint.2011.03.003, 2012.

Kurokawa, J., and Ohara, T.: Long-term historical trends in air pollutant emissions in Asia: Regional Emission inventory in ASia (REAS) version 3, Atmos. Chem. Phys., 20, 12761–12793, https://doi.org/10.5194/acp-20-12761-2020, 2020.

455 Li, L., Zhao, Q., Zhang, J., Li, H., Liu, Q., Li, C., Chen, F., Qiao, Y., and Han, J.: Bottom-up emission inventories of multiple air pollutants from open straw burning: A case study of Jiangsu province, Eastern China(Article), Atmos. Pollut. Res., 10, 501–507, https://doi.org/10.1016/j.apr.2018.09.011, 2019.

Li, M., Zhang, Q., Kurokawa, J. i., Woo, J.-H., He, K., Lu, Z., Ohara, T., Song, Y., Streets, D. G., Carmichael, G. R., Cheng, Y., Hong, C., Huo, H., Jiang, X., Kang, S., Liu, F., Su, H., and Zheng, B.: MIX: a mosaic Asian anthropogenic emission inventory under the international collaboration framework of the MICS-Asia and HTAP, Atmos. Chem. Phys., 17, 935–963, https://doi.org/10.5194/acp-17-935-2017, 2017.

Li, M., Fang, W., Li, J., and Yang, F.: The overall variation characteristics of Akedala atmospheric background station of pollutants, Env. Ecol., 1, 80–84, 2019.

Li, R., Mei, X., Chen, L., Wang, L., Wang, Z., and Jing, Y.: Long-Term (2005–2017) View of Atmospheric Pollutants in Central China Using Multiple Satellite Observations, Remote Sens-Basel, 12, 1041, https://doi.org/10.3390/rs12061041, 2020.

465 Liang, D., Wang, Y.-q., Wang, Y.-j., and Ma, C.: National air pollution distribution in China and related geographic, gaseous pollutant, and socio-economic factors, Env. Pollut., 250, 998–1009, https://doi.org/10.1016/j.envpol.2019.03.075, 2019.

Lin, W., Xu, X., Yu, D., Dai, X., Zhang, Z., Meng, Z., and Wang, Y.: Quality Control for Reactive Gases Observation at Longfengshan Regional Atmospheric Background Monitoring Station, Meteo. Mon., 35, 93–100, 2009.

Lin, W., Xu, X., Sun, J., Li, Y., and Meng, Z.: Characteristics of gaseous pollutants at Jinsha, a remote mountain site in Central China, Sci. 470 China, 41, 136–144, https://doi.org/10.1360/032010-521, 2011.

Lin, J. T., Martin, R. V. , Boersma, K. F. , Sneep, M., Stammes, P., Spurr, R., Wang, P., Van Roozendael, M., Clémer, K.and Irie, H.: Retrieving tropospheric nitrogen dioxide from the Ozone Monitoring Instrument: Effects of aerosols, surface reflectance anisotropy, and vertical profile of nitrogen dioxide, Atmos. Chem. Phys., 14, 1441–1461, https://doi:10.5194/acp-14-1441-2014, 2014.

Lin, J. T., Liu, M. Y., Xin, J. Y., Boersma, K. F., Spurr, R., Martin, R., and Zhang, Q.: Influence of aerosols and surface reflectance on 475 satellite NO2 retrieval: seasonal and spatial characteristics and implications for NOx emission constraints, Atmospheric Chemistry and Physics, 15, 11217–11241, https://doi:10.5194/acp-15-11217-2015, 2015.

Liu, M. Y., Lin, J. T., Boersma, K. F., Pinardi, G., Wang, Y., Chimot, J., Wagner, T., Xie, P., Eskes, H., Van Roozendael, M., Hendrick, F., Wang, P., Wang, T., Yan, Y. Y., Chen, L. L., and Ni, R. J.: Improved aerosol correction for OMI tropospheric NO$_2$ retrieval over East Asia: constraint from CALIOP aerosol vertical profile, Atmos. Meas. Techn., 12, 1–21, https://doi:10.5194/amt-12-1-2019, 2019.

480 Lin, W., Ma, Z., Pu, W., Gao, W., Ma, Q., and Yu, D.: Quality Control Methods for Atmospheric Composition Observations - Reactive Gases, in Meteorological industry standards in the People's Republic of China, 2019.

Liu, S., Jiang, X. T., Narcisse T. Lv, Chen, and Du, L.: Effects of NOx, SO$_2$ and RH on the SOA formation from cyclohexene photooxidation, Chemosphere, 216, 794–804, https://doi.org/10.1016/j.chemosphere.2018.10.180, 2019.

Meng, Z. Y., Xu, X. B., Yan, P., Ding, G. A., Tang, J., Lin, W. L., Xu, X. D., and Wang, S. F.: Characteristics of trace gaseous pollutants at 485 a regional background station in Northern China, Atmos. Chem. Phys., 9, 927–936, https://doi.org/10.5194/acp-9-927-2009, 2009.

Mi, C., and Qin, X.: Annual Report on Motor Vehicle Pollution Prevention and Control in China (2010), Yearbook of the People's Republic of China,0254–6108, 489, 2011.

Pandey, S. K., Kim, K.-H., Chung, S. Y. C., S.J. , Kim, M. Y., and Shon, Z. H.: Long-term study of NO_X behavior at urban roadside and background locations in Seoul, Korea, Atmos. Env., 42, 607–622, https://doi.org/10.1016/j.atmosenv.2007.10.015, 2008.

490   Qi, H., Lin, W., Xu, X., Yu, X., and Ma, Q.: Significant downward trend of SO_2 observed from 2005 to 2010 at a background station in the Yangtze Delta region, China, Science China Chemistry 55, 1451–1458, https://doi.org/10.1007/s11426-012-4524-y, 2012.

Qiu, Y. L., Ma, Z. Q., Lin, W.L., Quan, W. J., Pu, W.W., Li, Y.R., Zhou, L.Y., Shi, Q.F.: A study of peroxyacetyl nitrate at a rural site in Beijing based on continuous observations from 2015 to 2019 and the WRF-Chem model, Front. Environ. Sci. Eng., 14, 180-190, https://doi.org/10.1007/s11783-020-1250-0, 2020.

495   Resmi, C., Nishanth, T., Satheesh Kumar, M., Balachandramohan, M., and Valsaraj, K.: Long-Term Variations of Air Quality Influenced by Surface Ozone in a Coastal Site in India: Association with Synoptic Meteorological Conditions with Model Simulations, Atmosphere, 11, 193, https://doi.org/10.3390/atmos11020193, 2020.

Shen, J., He, L., Chen, P., Xie, M., Jiang, M., Chen, D., and Zhou, G.: Characteristics of Ozone Concentration Variation in the Northern Background Site of the Pearl River Delta, Eco. Environ. Sci., 28, 2006–2011, https://doi.org/10.16258/j.cnki.1674-5906.2019.10.010,
500   2019.

Shi, Y., Zhu, S., Li, L., Chen, Y., An, J., and Fu, Z.: Historical trends and spatial distributions of major air pollutants in the Yangtze River Delta, J. Lanzhou Univ. (Natural Sci.), 54, 184–191，199, https://doi.org/10.13885/j.issn.0455-2059.2018.02.007, 2018.

Squizzato, S., Masiol, M., Rich, D. Q., and Hopke, P. K.: $PM_{2.5}$ and gaseous pollutants in New York State during 2005–2016: spatial variability, temporal trends, and economic influences, Atoms. Env., 183, 209–224, https://doi.org/10.1016/j.atmosenv.2018.03.045, 2018.

505   Su, B., Liu, X., and Tao, J.: Background characteristics of SO_2, NO_X and CO in forest and alpine background areas of eastern China, Environ. Monit. China 15–21, 2013.

Sun, W., Shao, M., Granier, C., Liu, Y., Ye, C., and Zheng, J.: Long-Term Trends of Anthropogenic SO_2, NO_X, CO, and NMVOCs Emissions in China(Article), Earths Future, 6, 1112–1133, https://doi.org/10.1029/2018ef000822, 2018.

Swartz, J. S., Van Zyl, P. G., Beukes, J. P., Labuschagne, C. B., E. G. , Portafaix, T., Galy-Lacaux, C., and Pienaar, J. J.: Twenty-one years
510   of passive sampling monitoring of SO_2, NO_2 and O_3 at the Cape Point GAW station, South Africa, Atmos. Environ., 222, https://doi.org/10.1016/j.atmosenv.2019.117128, 2020a.

Swartz, J. S., Zyl, P. G. v., Beukes, J. P., Galy-Lacaux, C., Ramandh, A., and Pienaar, J. J.: Measurement report: Statistical modelling of long-term trends of atmospheric inorganic gaseous species within proximity of the pollution hotspot in South Africa, Atmos. Chem. Phys.,20, 10637–10665, https://doi.org/10.5194/acp-20-10637-2020, 2020b.

515   Tong, S., Hou, S., Zhang, Y. et al.: Comparisons of measured nitrous acid (HONO) concentrations in a pollution period at urban and suburban Beijing, in autumn of 2014. Sci. China Chem. 58, 1393–1402, https://doi.org/10.1007/s11426-015-5454-2, 2015.

US EPA：Quality Assurance Handbook for Air Pollution Measurement Systems, Volume II, Ambient Air Quality Monitoring Program, EPA-454/B-17-001, 2017.

Wan, Z., Ji, S., Liu, Y., Zhang, Q., Chen, J., and Wang, Q.: Shipping emission inventories in China's Bohai Bay, Yangtze River Delta, and
520   Pearl River Delta in 2018(Article), Mar. Pollution. Bulletin., 151, https://doi.org/10.1016/j.marpolbul.2019.110882, 2020.

Wang, H. L., Qiao, L. P., Lou, S. R., Zhou, M., Ding, A. J., Huang, H. Y., Chen, J. M., Wang, Q., Tao, S. K., Chen, C. H., Li, L., and Huang, C.: Chemical composition of PM2.5 and meteorological impact among three years in urban Shanghai, China, J. Clean. Prod., 112, 1302–1311, https://doi.org/10.1016/j.jclepro.2015.04.099, 2016.

Wang, L. Yuan,L, Zhang, X. L. , Jia, Y. T.：Characteristics and Source Apportionment of Black Carbon in Chengdu,Environ. Sci., 41 , 0250–
3301, https://doi.org/10.13227/j.hjkx.201908190,2020.

Wang, N., Lyu, X., Deng, X., Huang, X., Jiang, F., and Ding, A.: Aggravating O_3 pollution due to NOx emission control in eastern China,
Sci. Total. Environ., 677, 732–744, https://doi.org/10.1016/j.scitotenv.2019.04.388, 2019.

Wang, T., He, H., Xia, Z., Wu, M., and Zhang, Q.: Pollution characteristics of SO_2, NO_2, CO and O_3 in Nanjing in 2015, Chinese J. Environ.
Engi., 11, 4155–4161, 2017.

Wang, Y. Q.: MeteoInfo: GIS software for meteorological data visualization and analysis, Meteorol. Appl., 21, 360–368, 2014.
https://doi.org/10.1002/met.13

Xie, Z.: Global Financial Crisis Making a V-Shaped Fluctuation in NO_2 Pollution over the Yangtze River Delta, J. Meteorol. Res-Prc, 31,
438–447, https://doi.org/10.1007/s13351-017-6053-2, 2017b.

Xin, Y. J.，Wang, G. C., and Chen, L.: Identification of Long-Range Transport Pathways and Potential Sources of PM_{10} in Tibetan Plateau
Uplift Area: Case Study of Xining, China in 2014, Aerosol. Air. Qual. Res., 16, 1044–1054, https://doi.org/10.4209/aaqr.2015.05.0296,
2016.Xu, X., Lin, W., Yan, P., Zhang, Z., and Yu, X.: Long-term Changes of Acidic Gases in China's Yangtze Delta and Northeast Plain
Regions During 1994–2006, Adv. Clim. Change. Res., 195–201, 2008.

Xu, X., Yang, B., Shi, S., Wang, X., and He, H.: Analysis on the Current Situation of Acid Rain Pollution in Lin′an District of Hangzhou
City, J. Anhui. Agricul. sci., 47, 86–89，92, https://doi.org/10.3969/j.issn.0517-6611.2019.09.025, 2019.

Xue, R., Wang, S. L., Danran , Zou, Z., Chan, K. L., Valks, P., Saiz-Lopez, Alfonso, and Zhou, B.: Spatio-temporal variations in NO_2 and
SO_2 over Shanghai and Chongming Eco-Island measured by Ozone Monitoring Instrument (OMI) during 2008–2017, J. Clean. Prod., 258,
https://doi.org/10.1016/j.jclepro.2020.120563, 2020.

Yan, F., Chen, W., Jia, S., Zhong, B., Yang, L., Mao, J., Chang, M., Shao, M., Yuan, B., Situ, S., Wang, X., and Wang, D. C. X.: Stabilization
for the secondary species contribution to $PM_{2.5}$ in the Pearl River Delta (PRD) over the past decade, China: A meta-analysis, Atoms.
Env.,242, 117817, https://doi.org/10.1016/j.atmosenv.2020.117817, 2020.

Yang, B., and Luo, R.: Research progress of air pollution in Yangtze River Delta, Environ. Ecol., 1, 74–78, 2019.

Yang, J., Xin, J., Ji, D., and Zhu, B.: Variation Analysis of Background Atmospheric Pollutants in North China During the Summer of 2008
to 2011, Environ. Sci., 3693–3704, 2012.

Yang, Q.: Characteristics and Causes of Acid Rain Changes in Xiaoshan District, 2008–2017, Overs. Dig., 2018.

Yu, Y., Wang, Z., Cui, X., Chen, F., and Xu, H.: Effects of Emission Reductions of Key Sources on the $PM_{2.5}$ Concentrations in the Yangtze
River Delta, Environ. Sci. , 40, 11–23, https://doi.org/10.13227/j.hjkx.201804105, 2019.

Zhang, G., Jing, S.G., Xu, W.Y., Gao, Y.Q., Yan, C., Liang, L.L., Huang, C., Wang, H.L.: Simultaneous observation of atmospheric
peroxyacetyl nitrate and ozone in the megacity of Shanghai, China: Regional transport and thermal decomposition, Environ. Pollut., 274,
116570, https://doi.org/10.1016/j.envpol.2021.116570, 2021.

Zhao, B., Wang, S., Wang, J., Fu, J. S., Liu, T., Xu, J., Fu, X., and Hao, J.: Impact of national NOx and SO_2 control policies on particulate
matter pollution in China, Atmos. Env., 77, 453–463, https://doi.org/10.1016/j.atmosenv.2013.05.012, 2013.

Zhao, M., Qiao, T., Huang, Z., Zhu, M., Xu, W., Xiu, G., Tao, J., and Lee, S.: Comparison of ionic and carbonaceous compositions of $PM_{2.5}$
in 2009 and 2012 in Shanghai, China, Sci. Tot. Env., 536, 695–703, doi.org/10.1016/j.scitotenv.2015.07.100, 2015.

Zhao, P., Tuygun, G. T., Li, B., Liu, J., Yuan, L., Luo, Y., Xiao, H., and Zhou, Y.: The effect of environmental regulations on air quality: A long-term trend analysis of SO_2 and NO_2 in the largest urban agglomeration in Southwest China, Atmos. Pollut. Res., https://doi.org/10.1016/j.apr.2019.09.011, 2019.

Zhao, S., Liu, S., Hou, X., Cheng, F., Wu, X., Dong, S., and Beazley, R.: Temporal dynamics of SO_2 and NO_X pollution and contributions of driving forces in urban areas in China, Environ. Pollut., 242, 239–248, https://doi.org/10.1016/j.envpol.2018.06.085, 2018.

Zheng, S., Yi, H., and Li, H.: The impacts of provincial energy and environmental policies on air pollution control in China, Renew. Sust. Energ. Rev., 49, 386–394, https://doi.org/10.1016/j.rser.2015.04.088, 2015.

Zhou, D., Tian, X., Cai, Z., Wang, X., Li, Y., Liu, Y., and Jiang, F.: Evaluation of Ozone Change and Control Effects in Yangtze River Delta Region During G20 Submit, Environ. Monit. in China, 36, 41–49, https://doi.org/10.19316/j.issn.1002-6002.2020.02.06, 2020.

Department of Ecology and Environment of Zhejiang Province , Bulletin on the ecological environment of Zhejiang Province in 2006, http://sthjt.zj.gov.cn/art/2007/6/5/art_1201912_13471624.html, last access: 24 June 2021.

Department of Ecology and Environment of Zhejiang Province , Bulletin on the ecological environment of Zhejiang Province in 2007, http://sthjt.zj.gov.cn/art/2008/6/5/art_1201912_13471634.html, last access: 24 June 2021.

Department of Ecology and Environment of Zhejiang Province , Bulletin on the ecological environment of Zhejiang Province in 2008, http://sthjt.zj.gov.cn/art/2009/6/5/art_1201912_13471647.html, last access: 24 June 2021.

Department of Ecology and Environment of Zhejiang Province , Bulletin on the ecological environment of Zhejiang Province in 2009, http://sthjt.zj.gov.cn/art/2010/6/5/art_1201912_13471671.html, last access: 24 June 2021.

Department of Ecology and Environment of Zhejiang Province , Bulletin on the ecological environment of Zhejiang Province in 2010, http://sthjt.zj.gov.cn/art/2011/6/3/art_1201912_13471687.html, last access: 24 June 2021.

Department of Ecology and Environment of Zhejiang Province , Bulletin on the ecological environment of Zhejiang Province in 2011, http://sthjt.zj.gov.cn/art/2012/6/4/art_1201912_15028444.html, last access: 24 June 2021.

Department of Ecology and Environment of Zhejiang Province , Bulletin on the ecological environment of Zhejiang Province in 2012, http://sthjt.zj.gov.cn/art/2013/6/5/art_1201912_15028442.html, last access: 24 June 2021.

Department of Ecology and Environment of Zhejiang Province , Bulletin on the ecological environment of Zhejiang Province in 2013, http://sthjt.zj.gov.cn/art/2014/6/4/art_1201912_13471699.html, last access: 24 June 2021.

Department of Ecology and Environment of Zhejiang Province , Bulletin on the ecological environment of Zhejiang Province in 2014, http://sthjt.zj.gov.cn/art/2015/6/3/art_1201912_13471712.html, last access: 24 June 2021.

Department of Ecology and Environment of Zhejiang Province , Bulletin on the ecological environment of Zhejiang Province in 2015, http://sthjt.zj.gov.cn/art/2016/6/2/art_1201912_13471725.html, last access: 24 June 2021.

Department of Ecology and Environment of Zhejiang Province , Bulletin on the ecological environment of Zhejiang Province in 2016, http://sthjt.zj.gov.cn/art/2017/6/2/art_1201912_13471748.html, last access: 24 June 2021.

Department of Ecology and Environment of Jiangsu Province, Bulletin on the ecological environment of Jiangsu Province in 2006, http://hbt.jiangsu.gov.cn/art/2007/3/28/art_1649_3939925.html, last access: 24 June 2021.

Department of Ecology and Environment of Jiangsu Province, Bulletin on the ecological environment of Jiangsu Province in 2007, http://hbt.jiangsu.gov.cn/art/2008/3/28/art_1649_3939926.html, last access: 24 June 2021.

595 Department of Ecology and Environment of Jiangsu Province, Bulletin on the ecological environment of Jiangsu Province in 2008, http://hbt.jiangsu.gov.cn/art/2009/6/5/art_1649_3939927.html, last access: 24 June 2021.

Department of Ecology and Environment of Jiangsu Province, Bulletin on the ecological environment of Jiangsu Province in 2009, http://hbt.jiangsu.gov.cn/art/2010/6/22/art_1649_3939928.html, last access: 24 June 2021.

Department of Ecology and Environment of Jiangsu Province, Bulletin on the ecological environment of Jiangsu Province in 2010, http://hbt.jiangsu.gov.cn:8080/art/2011/6/2/art_1677_4232467.html, last access: 24 June 2021.

600 Department of Ecology and Environment of Jiangsu Province, Bulletin on the ecological environment of Jiangsu Province in 2011, http://www.jiangsu.gov.cn/art/2012/5/30/art_46750_2680095.html, last access: 24 June 2021.

Department of Ecology and Environment of Jiangsu Province, Bulletin on the ecological environment of Jiangsu Province in 2012, http://hbt.jiangsu.gov.cn/art/2013/6/5/art_1649_3939931.html, last access: 24 June 2021.

Department of Ecology and Environment of Jiangsu Province, Bulletin on the ecological environment of Jiangsu Province in 2013, 605 https://news.bjx.com.cn/html/20140604/515937.shtml, last access: 24 June 2021.

Department of Ecology and Environment of Jiangsu Province, Bulletin on the ecological environment of Jiangsu Province in 2014, https://huanbao.bjx.com.cn/news/20150604/626623.shtml, last access: 24 June 2021.

Department of Ecology and Environment of Jiangsu Province, Bulletin on the ecological environment of Jiangsu Province in 2015, http://www.jiangsu.gov.cn/art/2016/6/24/art_46580_2555980.html, last access: 24 June 2021.

610 Department of Ecology and Environment of Jiangsu Province, Bulletin on the ecological environment of Jiangsu Province in 2016, http://hbt.jiangsu.gov.cn/art/2017/4/15/art_1649_3939935.html, last access: 24 June 2021.

Department of Ecology and Environment of Shanghai city, Bulletin on the ecological environment of Shanghai city in 2006, https://link.sthj.sh.gov.cn/file/2006bulletin/contents.htm, last access: 24 June 2021.

Department of Ecology and Environment of Shanghai city, Bulletin on the ecological environment of Shanghai city in 2007, 615 https://link.sthj.sh.gov.cn/file/2007bulletin/index.htm. , last access: 24 June 2021.

Department of Ecology and Environment of Shanghai city, Bulletin on the ecological environment of Shanghai city in 2008, https://link.sthj.sh.gov.cn/file/2008bulletin/index.html, last access: 24 June 2021.

Department of Ecology and Environment of Shanghai city, Bulletin on the ecological environment of Shanghai city in 2009, https://link.sthj.sh.gov.cn/file/2009bulletin/index.html , last access: 24 June 2021.

620 Department of Ecology and Environment of Shanghai city, Bulletin on the ecological environment of Shanghai city in 2010, https://link.sthj.sh.gov.cn/file/2010bulletin/ch/cont.html , last access: 24 June 2021.

Department of Ecology and Environment of Shanghai city, Bulletin on the ecological environment of Shanghai city in 2011, https://link.sthj.sh.gov.cn/file/2011bulletin/index.html, last access: 24 June 2021.

Department of Ecology and Environment of Shanghai city, Bulletin on the ecological environment of Shanghai city in 2013, 625 https://link.sthj.sh.gov.cn/file/2014bulletin/index.html, last access: 24 June 2021.

Department of Ecology and Environment of Shanghai city, Bulletin on the ecological environment of Shanghai city in 2014, https://sthj.sh.gov.cn/assets/html/117972-02.pdf, last access: 24 June 2021.

Department of Ecology and Environment of Shanghai city, Bulletin on the ecological environment of Shanghai city in 2015, https://sthj.sh.gov.cn/hbzhywpt1143/hbzhywpt1144/20160329/0024-141845.html, last access: 24 June 2021.

630   Department of Ecology and Environment of Shanghai city, Bulletin on the ecological environment of Shanghai city in 2016, https://sthj.sh.gov.cn/hbzhywpt1143/hbzhywpt1144/20170601/0024-141846.html, last access: 24 June 2021.
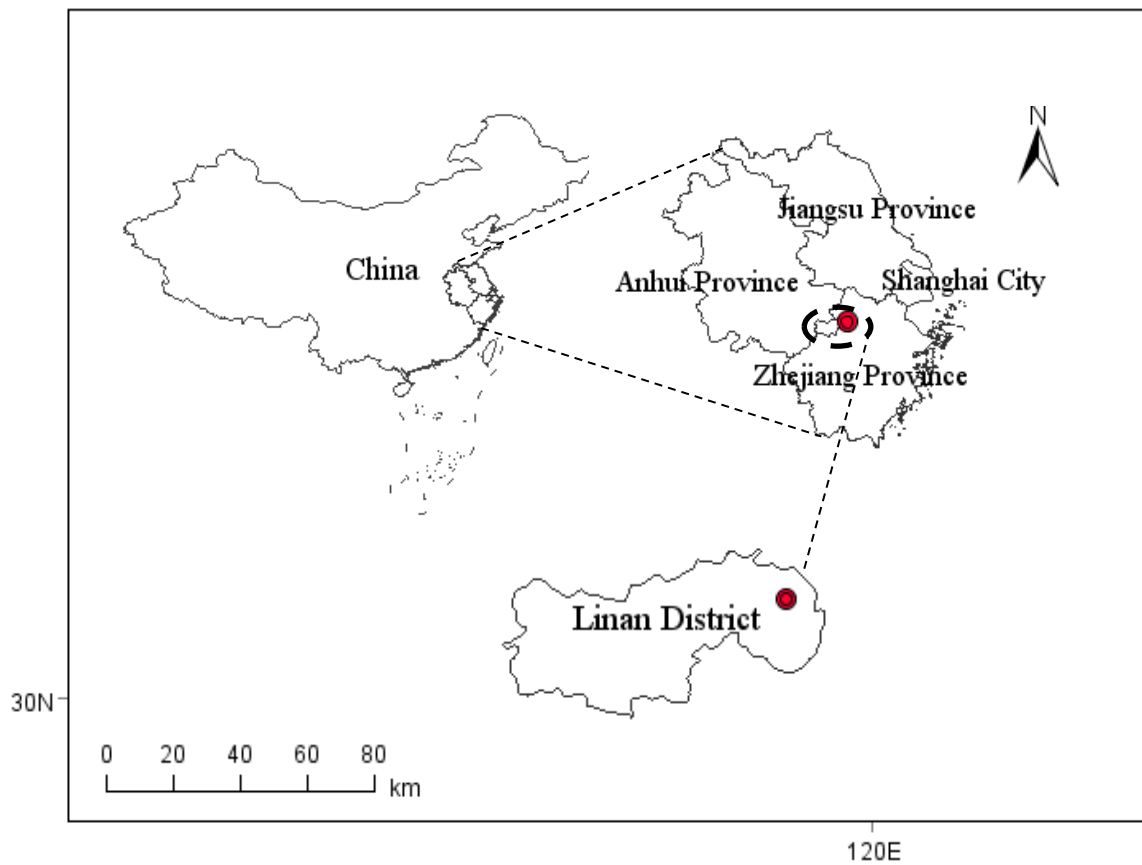
635   **Figure 1: Geographical location of LAN.**
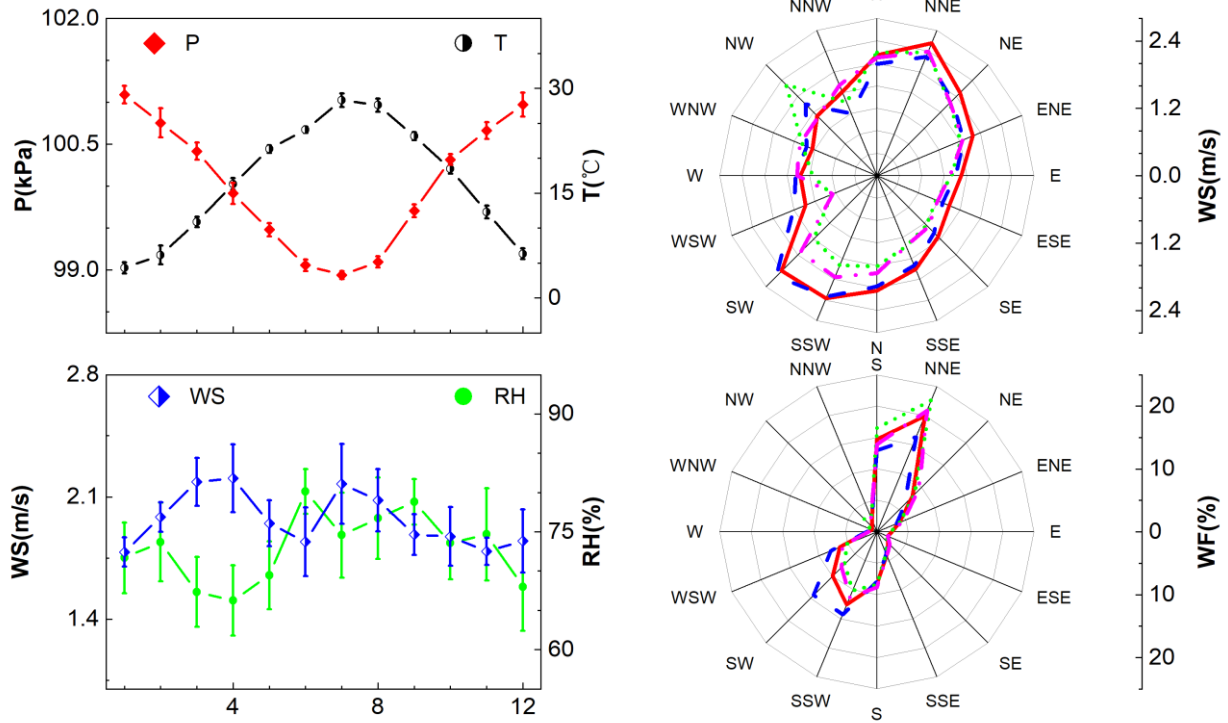
Figure 2: Average seasonal variations in air pressure (P), temperature (T), wind speed (WS), relative humidity (RH), and rose maps of wind speed (WS) and wind direction frequency (WF) at LAN during 2006–2016. In the rose maps of WS and WF, red solid represents spring, blue dash for summer, green short dot for autumn and magenta dash dot for winter.
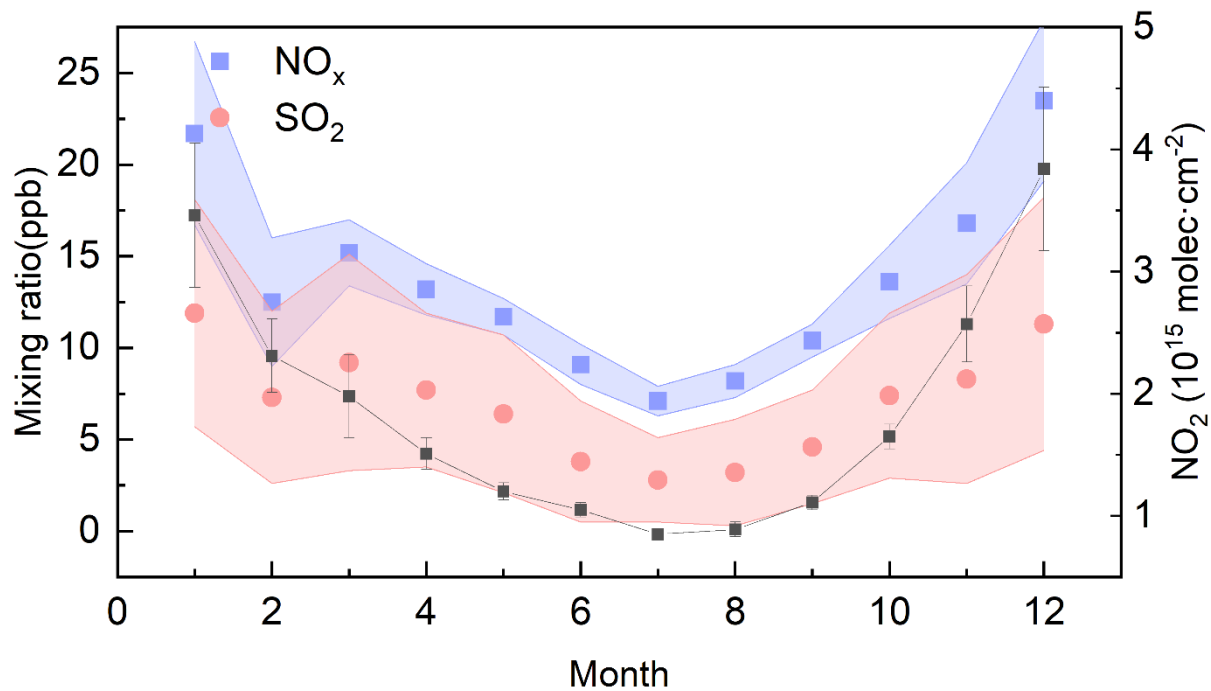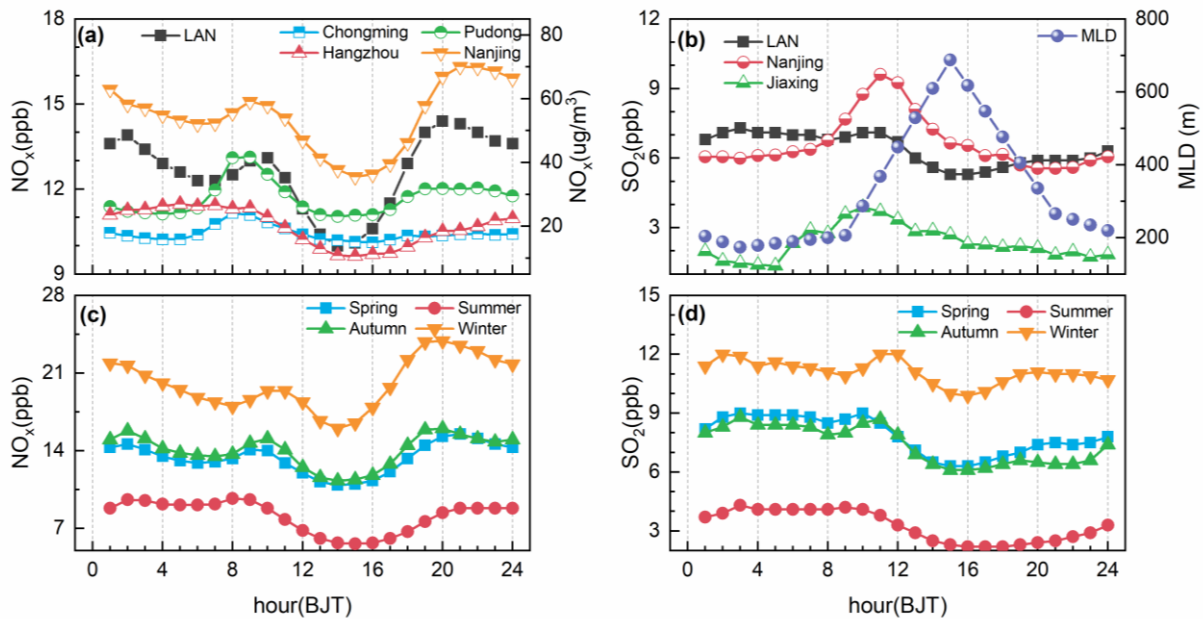
Figure 3: Monthly average NOₓ and SO₂ mixing ratios at LAN (left axis) and monthly tropospheric vertical column density of NO₂ (right axis) over 115.125° E–122.875° E and 27.125° N–35.875° N in the YRD during 2006–2016.

645

Figure 4: Annual average diurnal variations in NO_X (a, left axis) and in SO_2 (b, left axis) at LAN and its surrounding cities (NO_X, a, right axis; SO_2, b, left axis); seasonal average diurnal variations in NO_X (c, left axis) and SO_2 (d, left axis) at LAN. The average diurnal mixed layer depth (MLD; right axis) is also plotted in panel b.
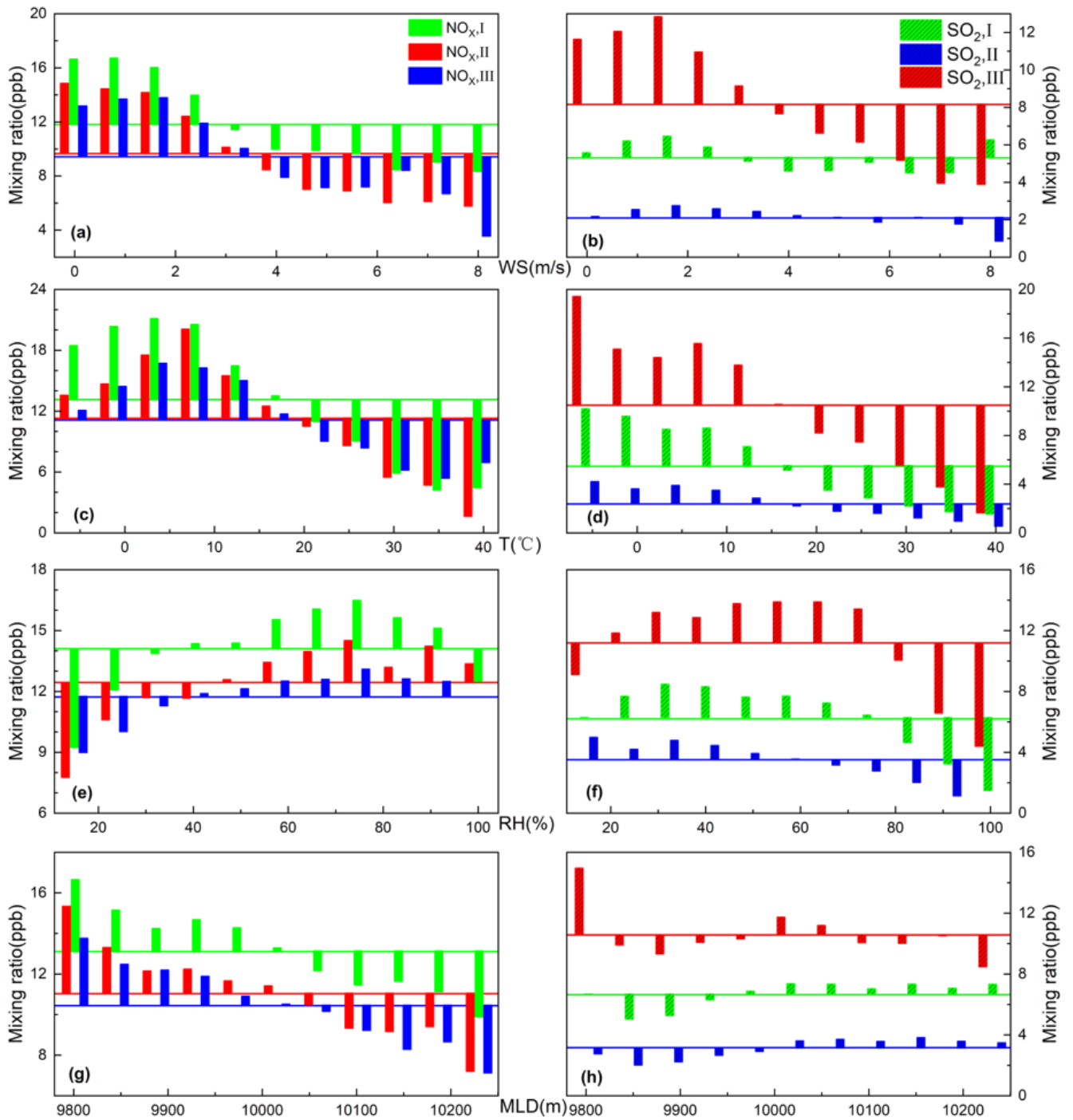
Figure 5: Variation characteristics of NOx and SO2 with wind speed (WS; a and b), temperature (T; c and d), relative humidity (RH; e and f), and the mixed layer depth (MLD; g and h) at LAN during period I (2006–2009), period II (2010–2013) and period III (2014–2016). The horizontal lines in the graph indicate the average values of NOx and SO2 for each period. Columns indicate changes relative to the corresponding mean values.
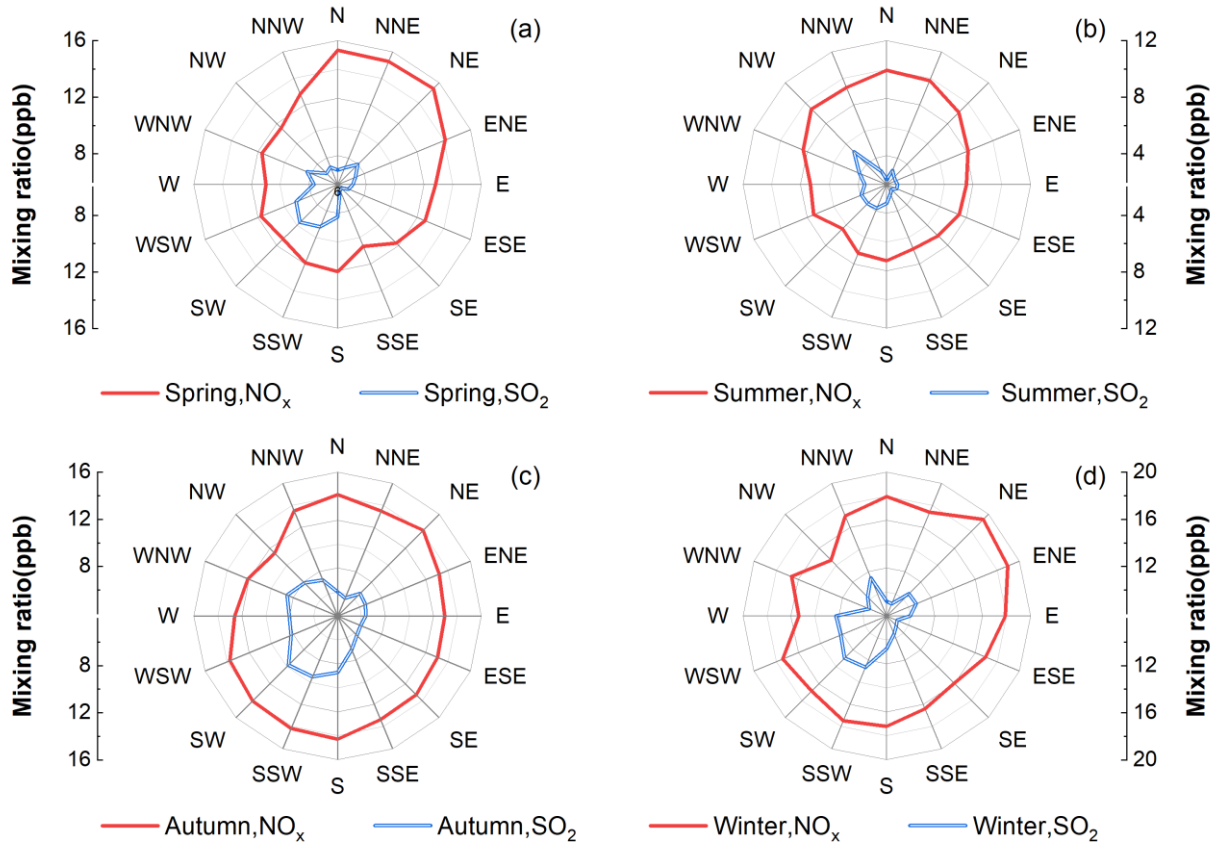
Figure 6: Seasonal distributions of NOX and SO2 concentrations in different wind directions.
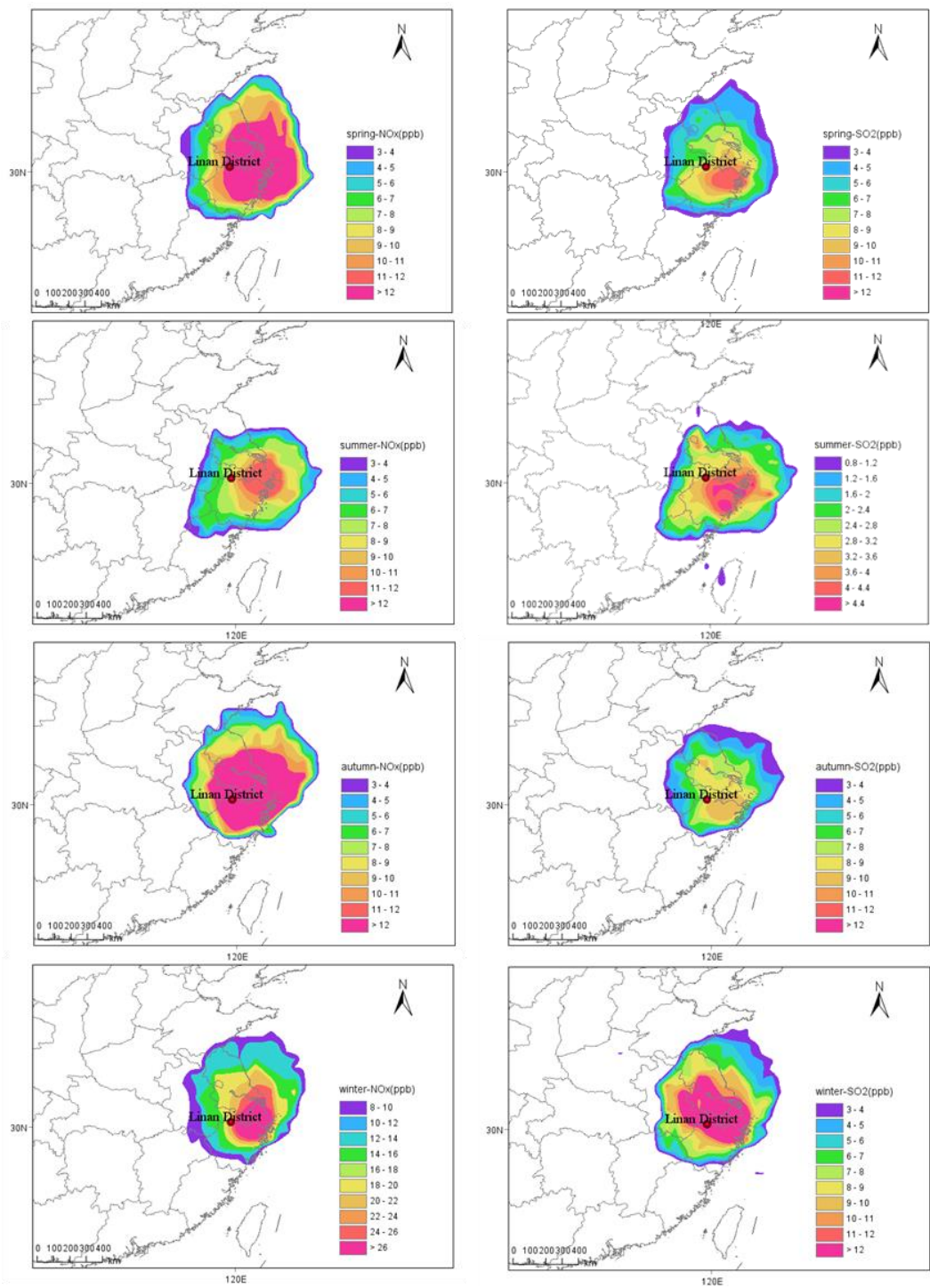
Figure 7: Potential source analysis of NOₓ and SO₂ in different seasons at LAN according to concentration weighted trajectory analysis.
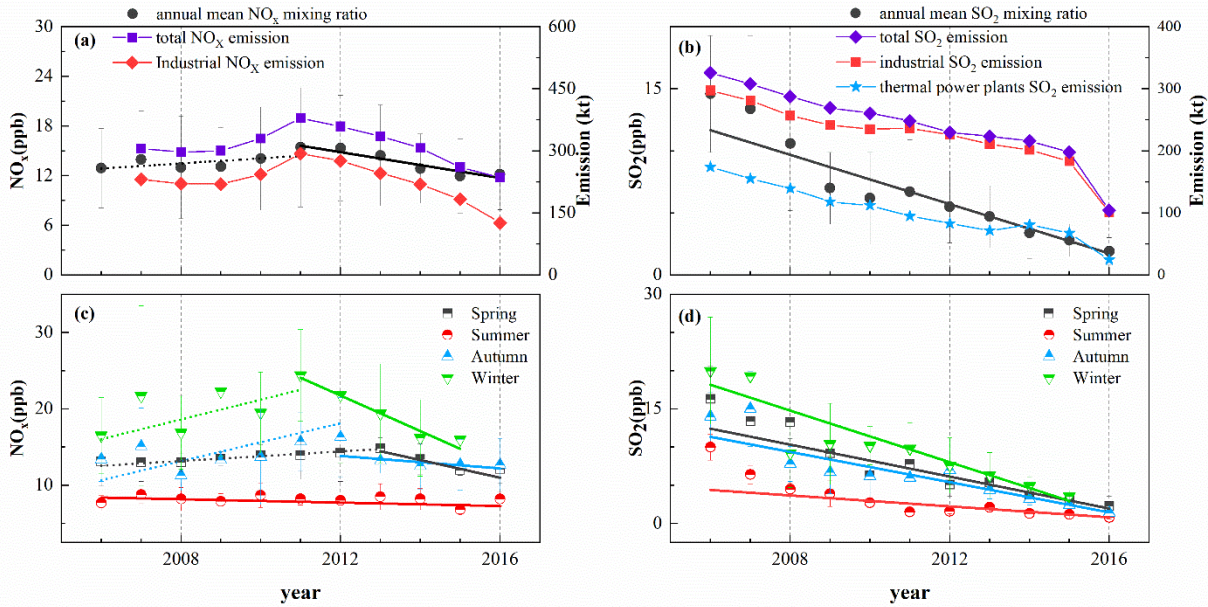
Figure 8: Annual mean NOx mixing ratio at LAN (left axis) compared with total NOx emission and industrial NOx emission in the YRD (a, right axis); annual mean SO₂ mixing ratio at LAN (left axis) compared with total SO₂ emission, industrial SO₂ emission, thermal power plants SO₂ emission in the YRD (b, right axis), seasonal average annual variation of NOx (c), and SO₂ (d) at LAN.
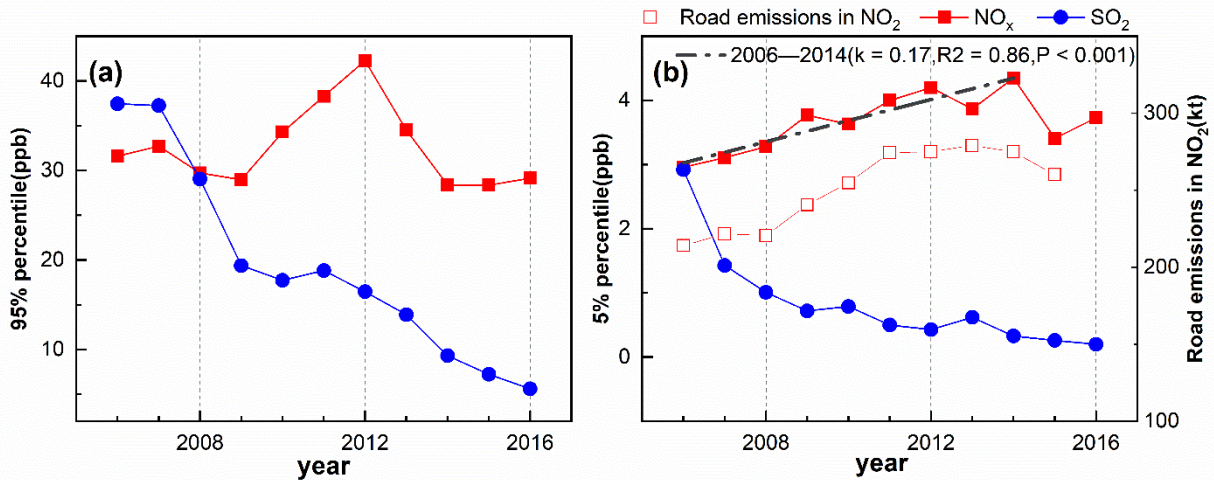
Figure 9: Annual variations in the 95 % percentile concentration (a) and the 5 % percentile concentration (b) of NOₓ and SO₂ at
**LAN; data of NO₂ road emissions in the YRD are obtained from the REASv3.2 data sets in the *Regional Emission inventory in Asia*
(Kurokawa and Ohara, 2020).**

**Figure 10: Reduced major axis regressions on the scatter plots of daily average SO₂ and NOₓ mixing ratios during three periods at
LAN.**

Figure 11: Average diurnal variations in NOX (a, c, e) and in SO2 (b, d, f) during period I (2006–2009), period II (2010–2013) and period III (2014–2016) at LAN.

Table 1 Statistics of NOx and SO₂ levels from 2006 to 2016 at LAN.

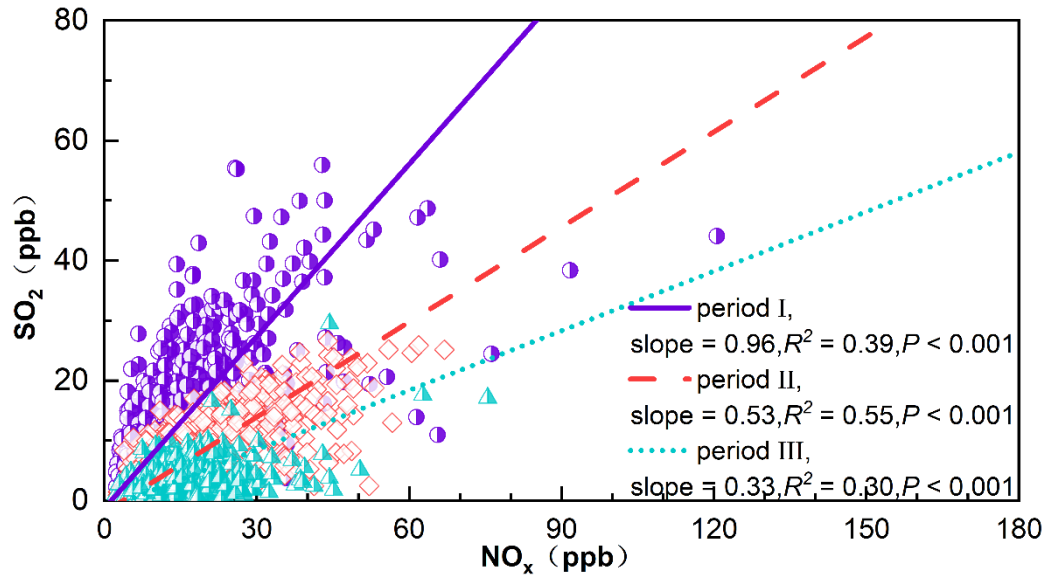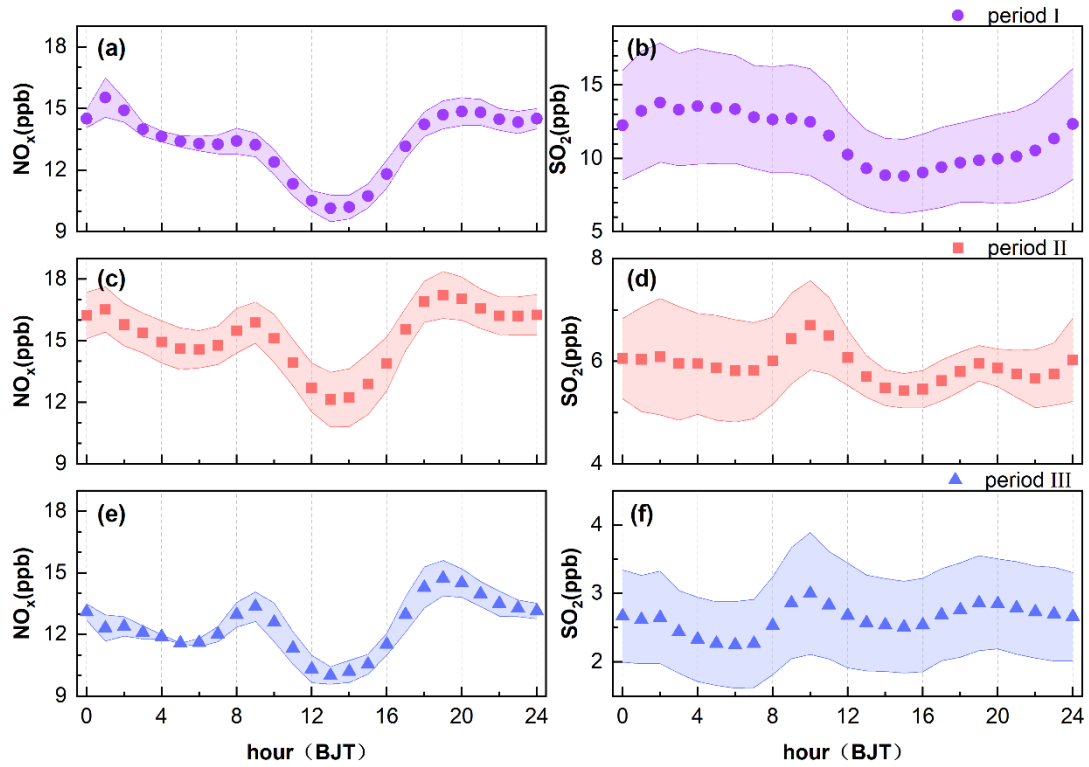| year	NO₂ (ppb)					NOx (ppb)					SO₂ (ppb)					SO₂/NOx
	Ave	Med	SD	Max	Min	Ave	Med	SD	Max	Min	Ave	Med	SD	Max	Min	
2006	12.1	10.9	4.2	19.9	6.0	12.9	11.5	4.8	22.0	6.5	14.6	13.8	4.7	24.7	8.4	1.13
2007	12.7	11.3	5.1	24.9	6.8	13.8	11.7	6.0	29.0	7.5	13.4	12.4	5.9	23.4	5.2	0.97
2008	12.0	10.8	5.0	22.5	6.2	13.0	11.3	6.2	27.9	6.6	10.6	10.6	5.4	19.9	3.7	0.82
2009	12.1	13.1	3.7	20.1	6.7	13.1	13.8	4.7	24.9	7.0	7.0	7.1	2.9	11.9	2.1	0.54
2010	12.5	11.6	5.1	24.5	6.5	14.1	12.5	6.2	29.3	7.6	6.2	5.7	3.7	14.9	1.9	0.44
2011	14.1	13.0	6.0	26.5	6.7	15.4	13.8	7.2	31.3	7.5	6.7	6.7	4.2	13.7	1.1	0.44
2012	13.8	14.8	5.4	22.2	5.6	15.4	15.8	6.4	26.8	5.9	5.5	6.0	2.9	9.3	1.3	0.36
2013	13.5	12.5	5.4	23.8	6.2	14.5	13.1	6.1	27.0	6.5	4.7	4.3	2.5	10.0	1.9	0.32
2014	12.1	11.8	3.7	18.8	7.0	12.9	12.4	4.2	20.2	7.3	3.4	3.0	2.1	8.6	1.0	0.26
2015	11.0	11.3	3.7	17.4	6.1	12.0	11.7	4.5	19.9	6.4	2.8	2.9	1.3	5.7	1.1	0.23
2016	11.1	10.7	3.4	16.8	6.8	12.2	11.4	4.3	19.8	7.2	1.9	1.6	1.1	3.7	0.6	0.16
Ave.	12.5	12.0	4.6	21.6	6.4	13.6	13.1	1.2	15.4	12.0	7.0	6.2	4.2	14.6	1.9	0.52

Ave: Average; Med: Median; SD: standard deviation; Max: maximum; Min: minimum.

31

Table 2 NO$_X$ and SO$_2$ mixing ratios observed at various atmospheric background stations.

Station	Latitude and longitude, altitude	Period of observation	NO$_X$/ppb	SO$_2$/ppb	SO$_2$/ NO$_X$	References
Lin'an*, Yangtze River Delta background station	30.3 °N,119.73 ° E, 138 m a.s.l.	2006.1–2016.12	13.6 ± 1.2	7.0 ± 4.2	0.55	This study
Shangdianzi*, North China Regional Background Station	40.39° N,117.07° E, 293.9 m a.s.l	2006.1–2006.12	12.7 ± 11.8	7.6 ± 10.2	0.60	(Meng et al., 2009)
Wuyishan, Eastern China Regional Background Station	27.58° N,117.72° E, 1139 m a.s.l	2011.3–2012.2	2.70	1.48	0.55	(Su et al., 2013)
Dinghushan, South China Regional Background Station	23.2° N,112.5° E, 100m a.s.l	2009.1–2010.12	13.6	6.5	0.48	(Chen, 2012)
Changbaishan, Northeast China Regional Background Station	42.4° N,117.5° E, 736 m a.s.l	2009.1–2010.12	4.7	2.1	0.45	(Chen, 2012)
Fukang, Northwest China Regional Background Station	44.3° N,87.9° E, 470 m a.s.l	2009.1–2010.12	8.3	2.2	0.27	(Chen, 2012)
Gonggar Mountain, Southwest China Regional Background Station	29.92° N,102.61° E, 3541 m a.s.l	2017.1–2017.12	0.90	0.19	0.21	(Cheng et al., 2019)
Jinsha, Central China Regional Background Station	29.63° N,114.2° E, 750 m a.s.l	2006.6–2007.7	5.6 ± 5.5	2.8 ± 5.5	0.5	(Lin et al., 2011)

* indicates that the site is also one of the World Meteorological Organization (WMO) Global Atmosphere Watch (GAW/WMO) atmospheric background stations

The date of NO$_2$ all above is converted to NO by a molybdenum NO$_2$-to-NO converter heated to about 325°C.

Table 3 Pearson correlations among NO$_X$, SO$_2$, and meteorological elements (daily average values).

		NO$_x$	SO$_2$	WS	T	RH	P	MLD
NO$_x$	annual	1	0.54*	−0.25*	−0.47*	−0.01	0.42*	−0.06*
	Spring		0.38*	−0.23*	−0.22*	0.09*	0.18*	−0.32*
	Summer		0.30*	−0.34*	−0.24*	0.04	0.25*	0.18*
	Autumn		0.46*	−0.28*	−0.36*	−0.06*	0.35*	−0.12*
	Winter		0.50*	−0.30*	0.06	0.09*	−0.07*	−0.22*
SO$_2$	annual		1	−0.09*	−0.34*	−0.41*	0.39*	0.08*
	Spring			−0.05	−0.04	−0.41*	0.17*	−0.05
	Summer			0.00	0.07*	−0.32*	0.11*	−0.02
	Autumn			−0.11*	−0.23*	−0.56*	0.31*	0.12*
	Winter			−0.13*	−0.07	−0.34*	0.17*	0.02

Two-tailed significance test was used.

*: Significant at 0.05 level of correlation

Table 4 Annual percentage changes in NO_X and SO_2 in various regions.

Location	Period	Base year	NO_X	SO_2
LAN, this study	2006–2016	2006	−0.49 %/yr	−8.27 %/yr
YRD, China	2006–2016	2006	−0.45 %/yr	−6.65 %/yr
Pearl River Delta, China	2000–2019	2006	−2.84 %/yr	−3.93 %/yr
Wuhan City, China	2005–2017	2006	+2.08%/yr	−9.46 %/yr
North China	2005–2014	2005	−3.34 %/yr	−0.78 %/yr
Northwest China	2010–2016	2010	+12.98%/yr	−13.06 %/yr
New York city in America	2005–2016	2005	−3.46 %/yr	−5.97 %/yr
Kraków city in Poland	2005–2020	2007	−2.21 %/yr	−3.43 %/yr*
Preila station in Lithuania	2005–2017	2006	−1.60 %/yr	−6.83 %/yr
Louis Trichardt in South Africa	2005–2017	2006	+1.85%/yr	−5.11 %/yr
Amersfoort city in South Africa	2005–2017	2006	+6.50%/yr	+2.95%/yr